Geol. Mag. **154** (*2*), *2017, pp. 217–236. © Cambridge University Press 2016*
doi:10.1017/S0016756815001120

Emplacement age and isotopic composition of the Prairie Lake carbonatite complex, Northwestern Ontario, Canada

FU-YUAN WU*†, ROGER H. MITCHELL‡, QIU-LI LI*, CHANG ZHANG* & YUE-HENG YANG*

*State Key Laboratory of Lithospheric Evolution, Institute of Geology and Geophysics, Chinese Academy of Sciences, P.O. Box 9825, Beijing 100029, China
‡Department of Geology, Lakehead University, Ontario, P7B 5E1, Canada

(*Received* 3 September 2015; *accepted* 18 December 2015; *first published online* 12 February 2016)

Abstract – Alkaline rock and carbonatite complexes, including the Prairie Lake complex (NW Ontario), are widely distributed in the Canadian region of the Midcontinent Rift in North America. It has been suggested that these complexes were emplaced during the main stage of rifting magmatism and are related to a mantle plume. The Prairie Lake complex is composed of carbonatite, ijolite and potassic nepheline syenite. Two samples of baddeleyite from the carbonatite yield U–Pb ages of 1157.2 ± 2.3 and 1158.2 ± 3.8 Ma, identical to the age of 1163.6 ± 3.6 Ma obtained for baddeleyite from the ijolite. Apatite from the carbonatite yields the same U–Pb age of ~1160 Ma using TIMS, SIMS and laser ablation techniques. These ages indicate that the various rocks within the complex were synchronously emplaced at about 1160 Ma. The carbonatite, ijolite and syenite have identical Sr, Nd and Hf isotopic compositions with a $^{87}Sr/^{86}Sr$ ratio of ~0.70254, and positive $\varepsilon_{Nd}(t)_{1160}$ and $\varepsilon_{Hf}(t)_{1160}$ values of ~+3.5 and ~+4.6, respectively, indicating that the silicate and carbonatitic rocks are co-genetic and related by simple fractional crystallization from a magma derived from a weakly depleted mantle. These age determinations extend the period of magmatism in the Midcontinent Rift in the Lake Superior area to 1160 Ma, but do not indicate whether the magmatism is associated with passive continental rifting or the initial stages of plume-induced rifting.

Keywords: U–Pb age, Sr–Nd–Hf isotopes, carbonatite, Prairie Lake complex, Midcontinent Rift.

1. Introduction

Alkaline and carbonatitic rocks are an important petrological record of anorogenic magmatism within cratons (Ernst & Bell, 2010), and hence these rocks provide invaluable information for deciphering the geodynamic evolution of these ancient continental blocks (Tappe *et al.* 2007). Taking the example of the North American continent, it is characterized by numerous anorogenic igneous suites subsequent to cratonization at ~1.8 Ga (Windley, 1993; Ernst & Bleeker, 2010). Among these, alkaline rock and carbonatite complexes occurring to the north of Lake Superior represent an important stage of Midcontinent rifting during Mesoproterozoic time (Rukhlov & Bell, 2010). The Midcontinent Rift has received much attention as it is one of the best-preserved Proterozoic intra-continental rifts, and potentially holds important clues as to the nature of Precambrian continental rifting (Van Schmus & Hinze, 1985; Palmer & Davis, 1987; Heaman *et al.* 2007; Hollings, Smyk & Cousens, 2012). Previous investigations indicated that the magmatism is diverse in lithology and composition, and includes the main stage of tholeiitic eruptions, lamprophyre, mafic–ultramafic intrusions (for example, the Duluth and Abitibi dykes), alkaline rock and carbonatite intrusions, rhyolite and related granophyre, etc. (Paces & Miller, 1993; Heaman *et al.* 2007; Vervoort *et al.* 2007; Hollings *et al.* 2007; Hollings, Smyk & Cousens, 2012; Bright *et al.* 2014). Previously, most studies have suggested that a plume (Keweenawan) was responsible for the rifting as a large volume (>10^6 km^3) of magma developed over a short period of ~20 Ma (Burke & Dewey, 1973; Ernst & Bell, 2010; Ernst & Bleeker, 2010). According to Heaman *et al.* (2007), the magmatism was initiated with lamprophyre and mafic magmatism (1150–1130 Ma), followed by mafic–ultramafic intrusions (1115–1110 Ma), the main rift magmatism (1108–1094 Ma) and synchronous alkaline–tholeiitic magmatism (1110–1100 Ma).

Within the Superior Province of the Canadian Shield, numerous Proterozoic alkaline rock and carbonatite complexes have been identified (Sage, 1983, 1987). One of these complexes, the Prairie Lake alkaline rock–carbonatite complex is situated northwest of Marathon, Ontario (49° 02′ N, 86° 43′ W), approximately 26 km from the shores of Lake Superior (Fig. 1). The complex has a surface area of 8.8 km^2 (Fig. 2) and consists predominantly of foidolitic and carbonatitic rocks emplaced in Archaean gneisses of the Superior craton along the Trans-Superior Tectonic Zone (Sage, 1987).

Previous geochronological studies have suggested that the Prairie Lake complex might have been emplaced between 1020 and 1200 Ma (see discussion in

†Author for correspondence: wufuyuan@mail.igcas.ac.cn

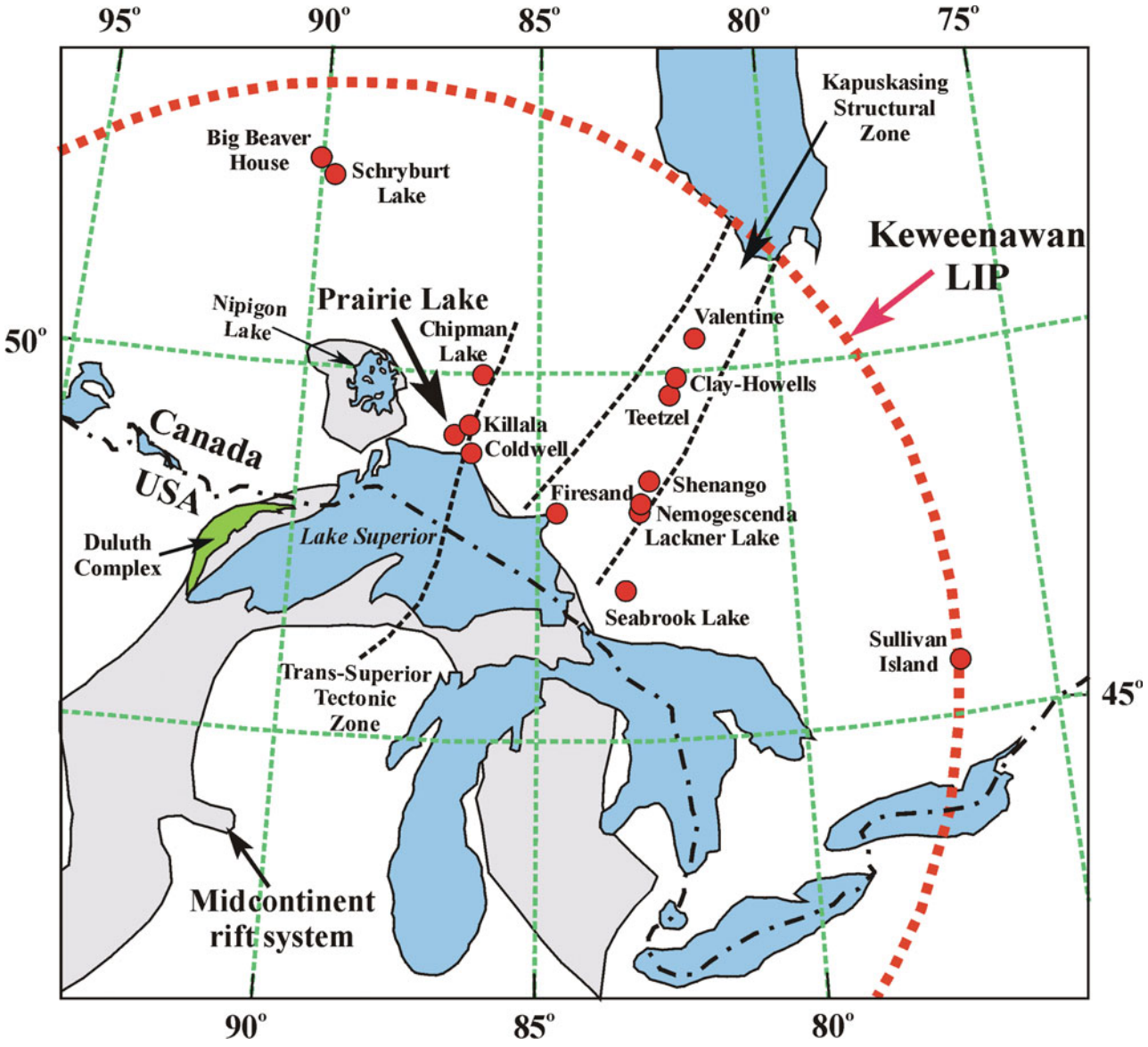

Figure 1. (Colour online) Distribution of the alkaline rock and carbonatite complexes within the Canadian part of the Midcontinent Rift. The spatial range of the proposed Keweenawan plume is also shown (modified from Ernst & Bell, 2010; Rukhlov & Bell, 2010).

Section 5 below). These investigations were not able to determine whether the different types of rocks in the complex were synchronously emplaced or not. In this study, we firstly present U–Pb geochronological data for baddeleyite and other related minerals to constrain accurately and precisely the time of emplacement of this complex, and then use Sr–Nd–Hf isotopic and trace-element data to consider the relationships between, and genesis of, the silicate and carbonatitic rocks of the complex.

2. Geological setting

The Midcontinent Rift is one of the most spectacular geological features of the North American continent, and extends from central Kansas, through Lake Superior and further east to Michigan (Fig. 1). It has been proposed that it represents an aborted or failed rift resulting from an upwelling mantle plume during

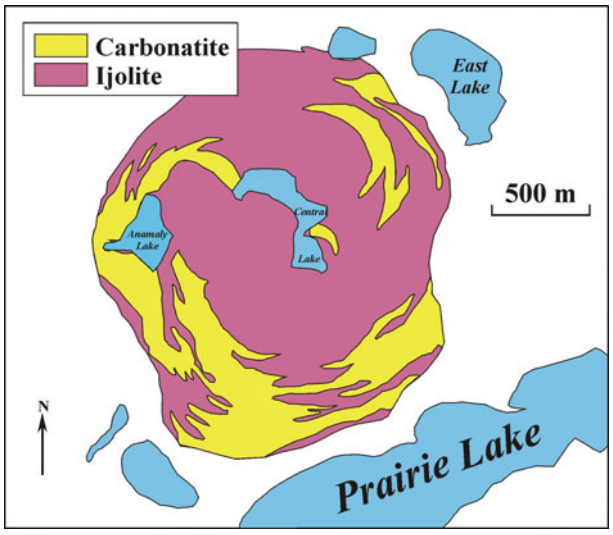

Figure 2. (Colour online) Geology of the Prairie Lake complex.

https://doi.org/10.1017/S0016756815001120 Published online by Cambridge University Press

Mesoproterozoic time at ~1.1 Ga (Burke & Dewey, 1973). The magmatism associated with the incipient rifting has been termed the Keweenawan Large Igneous Province (Ernst & Bell, 2010). The rift is characterized by a large volume (~1–2 × 10^6 km^3) of igneous material (Cannon, 1992; Merino *et al.* 2013), which includes tholeiitic volcanic rocks and related rhyolite and granophyre (Keweenawan Supergroup), mafic–ultramafic sills and intrusions, represented by the layered Duluth Complex in Minnesota (Paces & Miller, 1993), and alkaline rock and carbonatite intrusions in Canada (Fig. 1).

Within the Archaean rocks of the Quetico Subprovince of the Superior Province, numerous alkaline and carbonatitic rocks are distributed along the Trans-Superior Tectonic Zone and Kapuskasing Structural Zone, respectively (Fig. 1). Located within the former zone, four alkaline rock – carbonatite complexes (Coldwell, Chipman Lake, Killala Lake and Prairie Lake) have been recognized (Fig. 1). The Coldwell complex is one of the largest alkaline complexes in the world with an area of ~490 km^2, and is composed of subalkaline and alkaline gabbro, nepheline syenite, diverse contaminated syenites, ferroaugite syenite and A-type quartz syenites (Mitchell & Platt, 1978; Mitchell, Platt & Cheadle, 1983; Mitchell *et al.* 1993) with an emplacement age of ~1108 Ma (Heaman & Machado, 1992). The Killala complex consists of troctolite, gabbro, monzonite, syenite, nepheline monzonite–syenite and mafic–syenitic dykes, but lacks quartz syenites. Neither the Coldwell nor the Killala Lake complexes contain carbonatites. The Chipman Lake complex at the northern end of the Trans-Superior lineament consists of abundant carbonatitic dykes (Platt & Woolley, 1990).

2.a. Prairie Lake complex: geology

The limited outcrop of this small intrusion coupled with the significant modal heterogeneity of the rocks on a metre (or less) scale makes it difficult to construct a detailed geological outcrop map of the complex. Examination of drill cores also indicates significant complexity as particular petrographically defined units cannot be correlated even between closely sited drill holes. Regardless of these problems it is possible to recognize several broad petrographic units. On the basis of recent exploration activities (R. H. Mitchell, unpub. data; Purtich, Armstrong & Yassa, 2010), a schematic map is provided to show the distribution of these units (Fig. 2). They are described below in approximate order of intrusion.

2.a.1. Biotite pyroxenite and calcite carbonatite-(I)

Biotite pyroxenites are ultramafic coarse-grained, very friable rocks occurring principally in the NE sector of the complex (Fig. 2). The biotite pyroxenites are cut by many veins of very coarse-grained calcite carbonatite, here termed carbonatite-I. These veins and schlieren range in size from irregular segregations a few centimetres in length to large veins up to 1 m in width. This unit at its eastern extremity appears to have been intruded by carbonatite-(I) containing clasts of melanocratic ijolite. Carbonatite-(I) is a very friable coarse rock consisting of large interlocking calcite crystals with rare apatite present as aggregates of radial prisms. These rocks contain very little apatite or magnetite.

2.a.2. Ijolite series rocks

Much of the central region of the complex is occupied by diverse ijolite series rocks (Fig. 2). These are modally heterogeneous on a metre scale. Varieties present include: ijolite (pyroxene + nepheline), calcite mela-ijolite (silicocarbonatite or hollaite), mela-ijolite (pyroxene > nepheline with biotite and andradite–schorlomitic garnet) and wollastonite ijolite. Ijolite and mela-ijolite compose the bulk of this series. Several texturally distinct varieties can be recognized, although their relative disposition is unknown. The ijolitic rocks are notable in that they also contain accessory zirconolite, marianoite–wohlerite solid solutions and Zr-bearing titanite. Ijolite breccias are characteristic of the eastern parts of this unit.

A large area of wollastonite ijolite exposed in the southeastern portion of this unit has been shown by recent exploration trenching to be a megaxenolith incorporated in ijolitic breccia. Smaller clasts of wollastonite ijolite can be found in other parts of this breccia. The unit is clearly older than many of the other ijolites.

2.a.3. Potassic syenitic rocks

Mela-syenites, characterized by the presence of Na-poor potassium feldspar, nepheline and pyroxene, occur in the central and southern parts of the complex and are intimately mixed with ijolite-suite rocks (Fig. 2). The poor exposure prevents determination of their disposition but they are considered to be younger than the ijolites. Some of the malignites appear to be modally gradational into ijolite-suite rocks. The presence of a single non-perthitic feldspar plus nepheline indicates that these rocks are malignites (Mitchell & Platt, 1979) and *not* melanocratic nepheline syenites (*sensu lato)*. Characteristic accessory minerals are marianoite–wohlerite and Zr- and Nb-bearing titanite.

2.a.4. Heterogeneous carbonatite-(II)

This extensive complex unit forms a group of rocks extending from the northwest of the complex along the western margin to the SE margin of the complex (Fig. 2). The unit is characterized by great modal and textural diversity. Typically, the rocks are banded (or layered) on a centimetre to millimetre scale. Banding results from wide modal variations in the content of calcite, apatite, mica, olivine and magnetite. Fine-grained rocks are ‘interbedded’ with coarse-grained rocks. Large (up to 10 cm), rounded, coarse-grained

https://doi.org/10.1017/S0016756815001120 Published online by Cambridge University Press

apatite–mica-poor calcite carbonatite clasts can be found in the finer grained apatite carbonatites.

Modal layering in many places appears to be parallel to the margins of the complex. However, within any given area, the strike of the banding can vary significantly, and can range from near vertical to horizontal over a short distance. Extrapolation of the strike of layering from one area to another is not possible.

Carbonatite-(II), having more apatite and magnetite relative to carbonatite-I, contains numerous rounded clasts (centimetre to decimetre size) of ultramafic rocks derived from the deeper, and earlier-formed, parts of the complex. These clasts vary widely in mode and texture, and range from coarse-grained ijolite and biotite pyroxenite to micro-mela-ijolite and alnoitic lamprophyre. Some xenoliths of calcite ijolite contain flow-aligned prisms of calcite. The distribution of clasts is erratic, and clasts do not appear to be more abundant adjacent to the margin of the complex. Carbonatite-(II) also contains clasts of 'phoscorite' and 'disaggregated phoscorite'. Phoscorites, an imprecisely defined (Krasnova *et al.* 2004) but commonly used term, are considered in this work to be cumulate rocks consisting of magnetite + apatite + olivine and/or diopside with perovskite and/or pyrochlore.

Although there are continuous modal gradations, several varieties of carbonatite can be recognized as composing the heterogeneous carbonatite-(II) suite. These include: (a) coarse-grained apatite-poor calcite carbonatite; (b) olivine–apatite–magnetite calcite carbonatite with disaggregated phoscorite; (c) phlogopite–tetraferriphlogopite–magnetite–perovskite calcite carbonatite.

The modally variable olivine–apatite–magnetite calcite carbonatite composes most of the suite. Intrusive relationships between these diverse carbonatites have not been established and their distribution within the carbonatite-(II) suite is unknown. It is possible that the phlogopite perovskite-bearing carbonatites are younger than the olivine–apatite–magnetite carbonatites as the micas with respect to their composition are 'more evolved' than phlogopite in the latter rocks.

The carbonatite-(II) suite rocks contain a wide variety of minerals. Many of the oxide minerals and olivine are intergrown with other phases, and in particular with magnetite, and represent transported disaggregated cumulates.

The predominant minerals of carbonatite-(II) are: olivine ($Fo_{88–74}$), calcite (with 1–2 wt % SrO), fluorapatite (rare earth element (REE) and Sr-poor; <1 wt %), Ti-magnetite (3–12 wt % TiO_2), green pleochroic phlogopite–barian phlogopite and red pleochroic phlogopite–tetraferriphlogopite. Accessory minerals (1–5 vol. %) include Na–Ca-pyrochlore, U–Ta-bearing pyrochlore, Pb-pyrochlore, niobian zirconolite, perovskite–latrappite–loparite solid solution, baddeleyite and pyrite. Trace minerals (<1 vol. %) are thorianite, calzirtite, pyrrhotite, galena, cobaltian pentlandite, chalcopyrite, ancylite-(Ce), rhabdophane-(Ce) and Mn-ilmenite.

2.a.5. Dolomitic carbonatite

This unit is found only in a small area at the northern margin of the complex. It is bounded in the west by carbonatite-(II) and biotite pyroxenite in the east. Temporal relationships with these units are not established. This carbonatite appears to lack apatite and mica, but does contain REE-fluorocarbonates. It is considered to be a late-stage hydrothermal REE-enriched rock.

The Prairie Lake complex has been considered to be economically significant for uranium, niobium and tantalum deposits, owing to the occurrence of pyrochlore–betafite, wohlerite, perovskite and calzirtite in the carbonatite and ijolite, with apatite and/or wollastonite as potential by-products (Mariano, 1979; Mariano & Roeder, 1989; Purtich, Armstrong & Yassa, 2010).

3. Analytical methods

In this study, baddeleyite, perovskite, apatite, titanite and calcite were separated, hand-picked, mounted in epoxy resin and polished until the centres of the grains were exposed. Before any microprobe and isotopic analysis, back-scattered electron (BSE) images were obtained using a LEO1450VP scanning electron microscope (SEM), in order to assess internal compositional variation and textures, and identify potential target sites for compositional, U–Pb and Sr–Nd–Hf analyses. All analyses were conducted at the Institute of Geology and Geophysics, Chinese Academy of Sciences, Beijing.

3.a. Major- and trace-element analyses

Major-element compositions of the minerals were obtained using a JEOL–JAX8100 electron microprobe with a 15 kV accelerating potential and a 12 nA beam current. Counting times were 20 s. Total Fe is expressed as FeO_T. The analytical uncertainties are within 2 % for those major elements with concentrations >5 %, but ~10–20 % for other elements owing to their low concentrations.

Trace-element, including REE, compositions were obtained using an Agilent 7500a Q–ICP–MS (quadruple inductively coupled plasma mass spectrometer), which is equipped with a 193 nm excimer ArF laser ablation system (GeoLas Plus). The elemental concentrations were calculated using GLITTER 4.0 and calibrated using internal standards of ^{43}Ca for apatite, calcite, perovskite and titanite, and ^{90}Zr for baddeleyite. NIST610 was used as an external reference material during analyses (Griffin *et al.* 2008).

3.b. *In situ* U–Pb analyses of baddeleyite by SIMS

Baddeleyite U–Pb analyses were performed using a CAMECA 1280 ion microprobe located at the Institute of Geology and Geophysics in Beijing. A detailed description of the analytical procedure can be found in Li *et al.* (2010). In contrast to other U-bearing minerals, such as zircon, monazite and titanite, *in situ* secondary

https://doi.org/10.1017/S0016756815001120 Published online by Cambridge University Press

ion mass spectrometry (SIMS) U–Pb age determination of baddeleyite is difficult owing to crystal orientation effects which bias the $^{206}Pb/^{238}U$ ratio (Wingate & Compston, 2000). Therefore, the oxygen flooding technique was applied during this study as it has been shown that this technique can significantly reduce the orientation effects (Li *et al.* 2010). During analysis, Pb/U ratios were calibrated with a power law relationship between Pb/U and UO_2/U relative to a Phalaborwa baddeleyite standard which has a U–Pb age of 2059.6 Ma (Heaman, 2009). The measured Pb isotopic compositions were corrected for common Pb using non-radiogenic ^{204}Pb measured. Small corrections are insensitive to the choice of common Pb composition, and hence an average of the present-day crustal composition (Stacey & Kramers, 1975) is applied for the common Pb assuming that this originates mainly from surface contamination introduced during sample preparation. Uncertainties of individual analyses are reported at a 1σ level, and mean ages for pooled Pb/Pb analyses are quoted with a 95 % confidence interval using the Isoplot/Ex v. 3.0 program (Ludwig, 2003).

3.c. *In situ* Sr–Nd–Hf isotopic analyses by laser ablation

The *in situ* Sr–Nd–Hf isotopic analyses were conducted using a Neptune MC-ICP-MS (multi-collector inductively coupled plasma mass spectrometer) instrument. Detailed analytical protocols are given by Yang *et al.* (2008, 2009) and Wu *et al.* (2006); only a brief summary is given here.

The Sr isotopic data were acquired in static, multi-collector mode with low resolution using eight Faraday collectors and the mass configuration array from ^{83}Kr to ^{88}Sr, monitoring Kr and Rb (Yang *et al.* 2009). The key point of *in situ* Sr isotopic data acquisition is corrections for interfering elements. During this study, these effects were accounted for in the order of Kr, Yb^{2+}, Er^{2+} and Rb (Yang *et al.* 2009), but interferences from Fe dioxides, Ga and Zn oxides, $^{176}Lu^{2+}$ and $^{176}Hf^{2+}$ are not considered owing to their very low signals during analyses. In order to avoid potential matrix-mismatch effects, the in-house standards of LAP and SAP (apatite), NW-1 and Hainan coral (calcite), and AFK (perovskite) were used for the external correction of $^{87}Sr/^{86}Sr$ ratios. The $^{87}Sr/^{86}Sr$ ratios of these standards obtained by using thermal ionization mass spectrometry (TIMS) solution techniques are 0.71138 ± 2 (LAP), 0.72652 ± 1 (SAP), 0.70250 ± 2 (NW-1), 0.70918 ± 2 (Hainan coral) and 0.70335 ± 4 (AFK), respectively (Wu *et al.* 2013). However, $^{87}Rb/^{86}Sr$ ratios were not corrected as this ratio is extremely low for the analysed apatite, calcite and perovskite, and hence has no effect on the initial $^{87}Sr/^{86}Sr$ ratio of the samples investigated.

The *in situ* Nd isotope analytical technique is similar to that for the Sr isotope analysis as described above. The most important difficulty needed to be overcome during analysis is the interference of ^{144}Sm on ^{144}Nd, since our previous study shows that the influence of ^{142}Ce on ^{142}Nd is insignificant (Yang *et al.* 2008). For the correction of ^{144}Sm interference on ^{144}Nd, a method proposed by McFarlane & McCulloch (2007) was applied during this study. Similarly, the in-house standards of AP1 and AP2 (apatite), and AFK (perovskite) were used for the external corrections of $^{147}Sm/^{144}Nd$ and $^{143}Nd/^{144}Nd$ in order to overcome the potential matrix-mismatch effects. The reported $^{147}Sm/^{144}Nd$ and $^{143}Nd/^{144}Nd$ ratios by TIMS analysis are 0.0825 and 0.511352 ± 24 for AP1, 0.0764 and 0.510007 ± 30 for AP2, and 0.0659 and 0.512609 ± 27 for AFK, respectively (Wu *et al.* 2013; Yang *et al.* 2014).

In situ Hf isotopic analysis of baddeleyite is much easier than that for Sr and Nd isotopes. The isobaric interference of ^{176}Lu on ^{176}Hf is not significant owing to the extremely low $^{176}Lu/^{177}Hf$ of the minerals investigated (normally < 0.001). However, interference of ^{176}Yb on ^{176}Hf is not negligible. During this analysis, the mean $^{173}Yb/^{172}Yb$ ratio of an individual spot was used to calculate the fractionation coefficient (β_{Yb}), and then this coefficient was used to calculate the interference of ^{176}Yb on ^{176}Hf (Wu *et al.* 2006). Zircon standards 91500 and GJ-1 were used for external calibration. During analytical sessions, the $^{176}Hf/^{177}Hf$ value obtained for 91500 was 0.282302 ± 36 (2SD, n = 37), which is similar to the TIMS value of 0.282305 (Wu *et al.* 2006). As an unknown sample during analyses, the GJ-1 zircon gives a $^{176}Hf/^{177}Hf$ ratio of 0.282004 ± 7 (2σ, n = 20), agreeing well with the recommended value (0.282000 ± 5) from the literature (Morel *et al.* 2008). However, in order to avoid the potential matrix effect between zircon and baddeleyite, the Phalaborwa baddeleyite (Phala-1) was analysed during analyses and yielded a $^{176}Hf/^{177}Hf$ ratio of 0.281200 ± 16 (2σ, n = 7), which is slightly lower than the previously reported values by TIMS (0.281229 ± 11) and laser ablation (0.281238 ± 12) analyses (Wu *et al.* 2006, 2011). Therefore, a small correction of 30 ppm was applied for the analysed baddeleyite.

4. Analytical results

4.a. Mineral compositions

In this study, 8 carbonatite, 25 ijolite, 4 syenite and 1 gneissic xenolith samples were selected for mineral separation and further geochemical analysis. Only apatite, calcite, baddeleyite, titanite and perovskite were selected for compositional and isotopic analyses. Mineral compositions are listed in the online Supplementary Material available at http://journals.cambridge.org/geo and the REE distribution patterns are shown in Figure 3. Apatite occurs in all the rocks, and does not show any significant difference in composition (53.7–56.5 wt % CaO, 39.1–43.0 wt % P_2O_5, 0.1–1.3 wt % SiO_2). In terms of trace elements, apatite is characterized by high Sr (3760–7610 ppm) and low Ba (10–36 ppm) contents (Fig. 4a, b). The chondrite-normalized REE distribution pattern is steep, with only the apatite from the county rock (X-1) showing significant depletions in light REEs (LREEs) (Fig. 3a).

https://doi.org/10.1017/S0016756815001120 Published online by Cambridge University Press

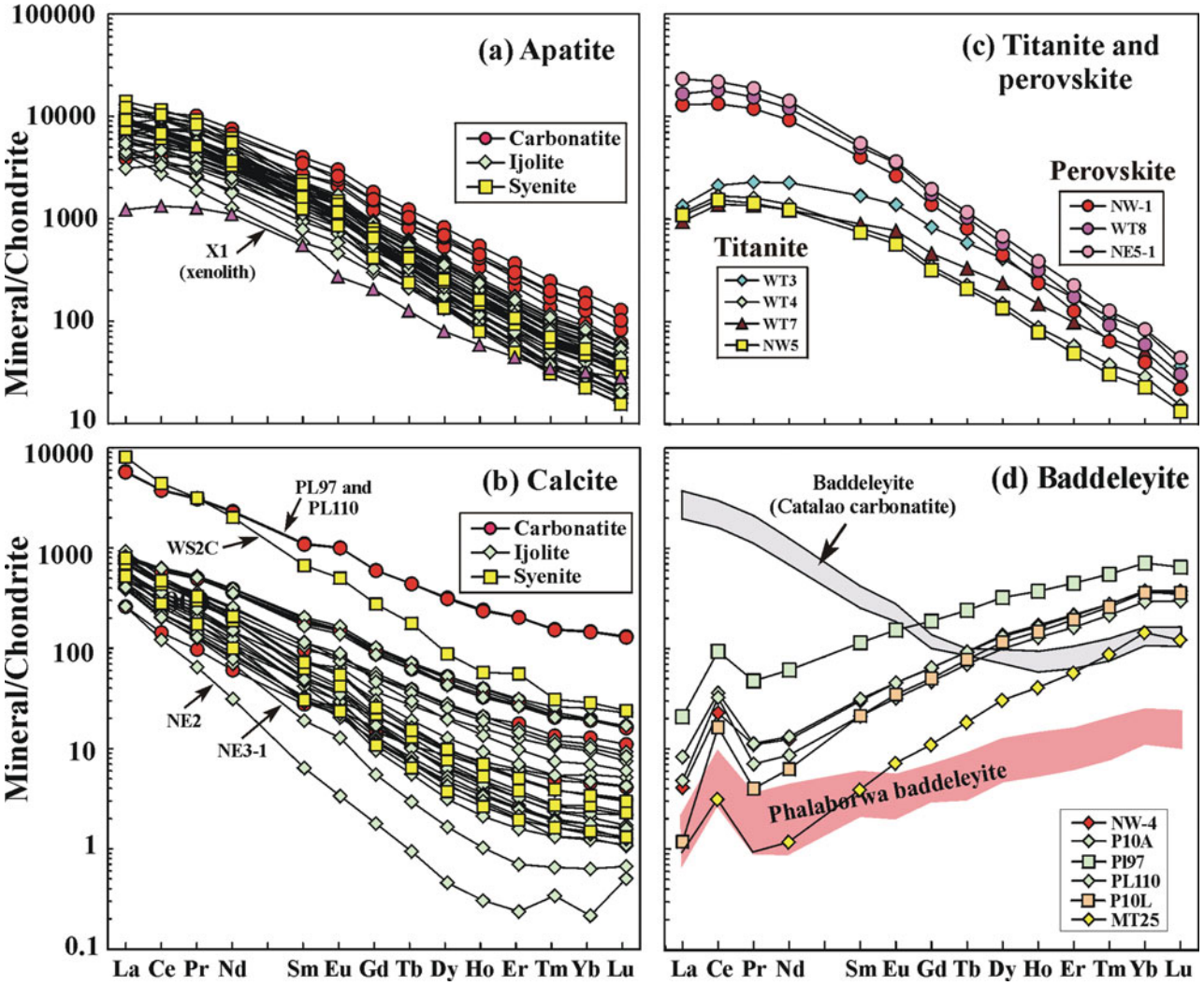

Figure 3. (Colour online) Rare earth elemental distribution patterns of (a) apatite; (b) calcite; (c) titanite and perovskite; and (d) baddeleyite. Data sources: Phalaborwa baddeleyite – Wu *et al.* (2011); Catalao carbonatite baddeleyite – unpublished data (F. Y. Wu).

Calcite is the major mineral of carbonatite-(II) (hereafter referred to simply as carbonatite), but is also common in the calcite ijolite and syenites. As shown in Figure 3b, calcite from different samples shows variable REE distribution patterns, but no distinct differences can be identified between the different rock types. Most calcites are characterized by a steep REE distribution pattern with high LREE and low heavy REE (HREE) abundances. Compared to apatite, calcite has higher Sr (6590–89 690 ppm) and Ba (201–7394 ppm) (Fig. 4a, b), but lower Nb, Hf, Pb, Th and U concentrations (Fig. 4c).

Titanite from the ijolite contains ~29 wt % SiO_2, 31.2–33.6 wt % TiO_2 and 26.1–26.5 wt % CaO with minor Al_2O_3 (0.3–0.7 wt %) and FeO (1.5–2.0 wt %). With respect to trace elements, titanite has high Nb (5909–22 485 ppm), Ta (171–1241 ppm), Zr (4978–18 465 ppm) and Sr (721–1135 ppm) with low Rb (0.1–0.9 ppm). Titanite has lower contents of REEs, and greater depletion of La and Ce than apatite (Fig. 3c). The perovskite is mostly euhedral with a grain size of ~200 μm. The perovskite exhibits a variable composition. Perovskite from the ijolite (NE3-1, NE5-1, WT2 and WT8) has 52.5–54.6 wt % TiO_2 and 36.8–38.1 wt % CaO with minor FeO_T (1.1–1.5 wt %) and Na_2O (0.4–0.5 wt %). However, perovskite from the carbonatite (NW-1) has a higher concentration of Nb_2O_5 (~16 wt %) with TiO_2 of 37.2–38.2 wt %, CaO of 30.8–32.2 wt % and minor FeO (3.6–3.8 wt %) and Na_2O (2.9–3.6 wt %). With respect to trace elements, the perovskites are characterized by high concentrations of Sr (2003–3764 ppm) and Ta (369–791 ppm), but low Zr (139–390 ppm) and Hf (3.4–8.9 ppm) and minor Rb (0.1–0.7 ppm). The REE distribution patterns show extreme LREE enrichment with La abundances of about 13 000–23 000 times higher than those of chondrites (Fig. 3c).

Baddeleyite occurs in both the carbonatite and ijolite and contains 94.9–98.6 wt % ZrO_2 with minor HfO_2 (0.4–0.6 wt %). The baddeleyites contain significant amounts of Nb (3938–11 035 ppm) and Ta (285–2880 ppm). In terms of REE distribution patterns, the baddeleyite is characterized by depletion of LREEs and enrichment of HREEs with significant positive Ce anomalies (Fig. 3d). Baddeleyites from the ijolite (P10L and MT25) have lower REE concentrations

https://doi.org/10.1017/S0016756815001120 Published online by Cambridge University Press

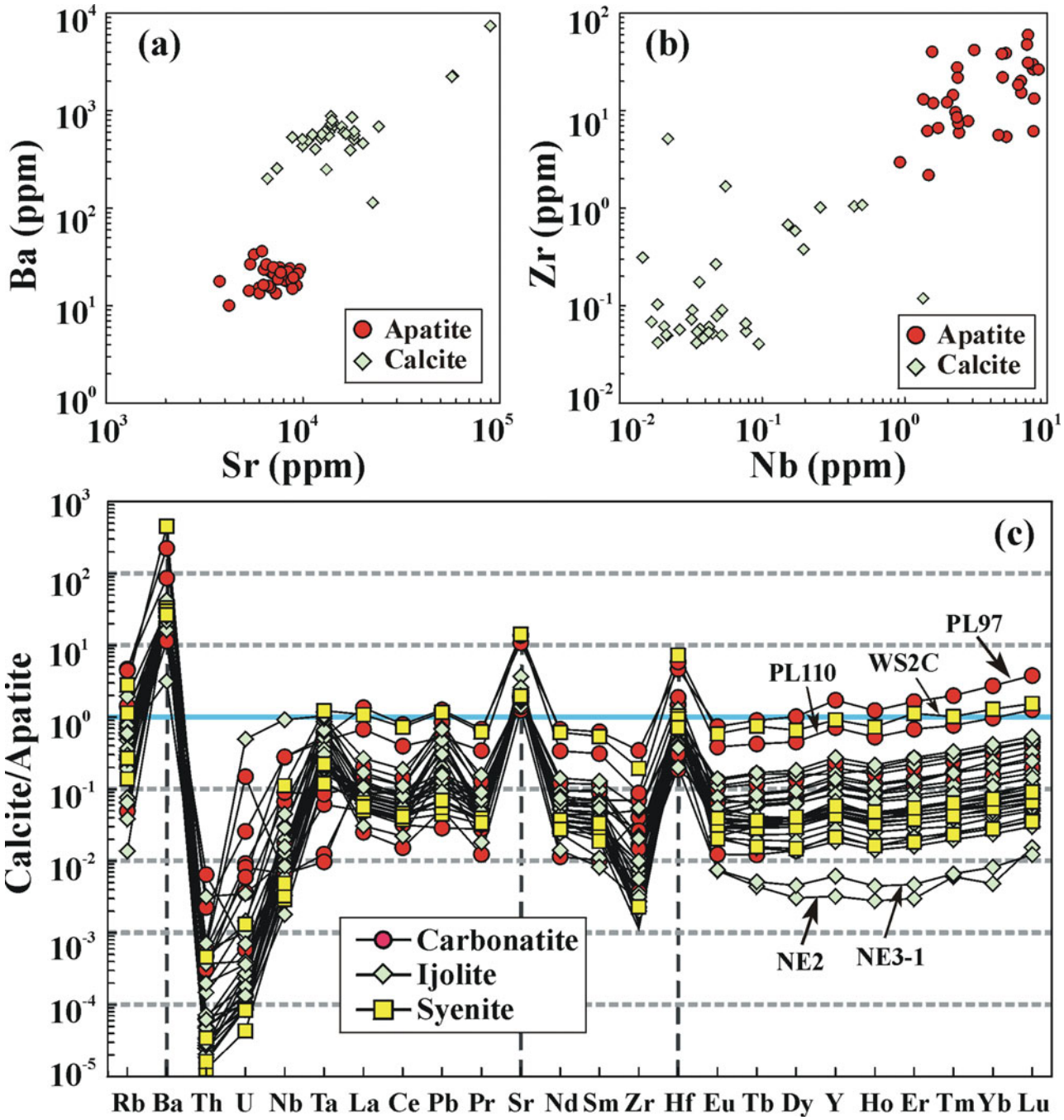

Figure 4. (Colour online) (a) Ba v. Sr and (b) Zr v. Nb variations between apatite and calcite, and (c) trace elemental ratios of calcite and apatite from different rock types.

than those from the carbonatite (NW-4, P10A, PL97 and PL110). Compared with the Phalaborwa complex (Wu *et al.* 2011), the baddeleyite in the Prairie Lake complex has much higher REE concentrations, especially for the HREEs, but contains much lower LREEs than in the niobium-rich Catalao carbonatite in Brazil (Fig. 3d).

4.b. Baddeleyite U–Pb ages

Six samples of baddeleyite were extracted from the carbonatite and ijolite, but only four were selected for U–Pb age determination (Table 1). These baddeleyites have a grain size of ~100 μm. The U concentrations are 228–2400 ppm for NW-4, 178–2210 ppm for P10A, 0.4–130 ppm for MT25 (mostly < 5 ppm) and 125–2049 ppm for P10L, respectively. For the carbonatite, the obtained ^{207}Pb–^{206}Pb weighted average ages are 1157.2 ± 2.3 Ma for NW-4 and 1158.2 ± 3.8 Ma for P10A (Fig. 5a, b). Baddeleyite from the ijolite (MT25) has a much lower U content, making age determination difficult, although a ^{207}Pb–^{206}Pb weighted average age of 1170 ± 18 Ma was obtained (Fig. 5c). However, baddeleyite from an ijolite clast in sample P10L within the carbonatite yielded an age of 1163.6 ± 3.6 Ma (Fig. 5d).

https://doi.org/10.1017/S0016756815001120 Published online by Cambridge University Press

Table 1. Baddeleyite U–Pb isotopic data by SIMS analysis

Sample/ spot no.	[U] ppm	[Th] ppm	[Pb] ppm	Th/U meas.	$^{207}Pb/^{235}U$	±σ %	$^{206}Pb/^{238}U$	±σ %	$^{207}Pb–^{206}Pb$	±σ	$^{207}Pb–^{235}U$	±σ	$^{206}Pb–^{238}U$	±σ
NW-4@1	982	7	228	0.007	2.325	3.59	0.215	3.58	1161.6	5.1	1219.8	25.8	1253.0	40.9
NW-4@2	617	5	134	0.009	2.178	3.60	0.201	3.58	1160.7	6.7	1174.1	25.4	1181.3	38.8
NW-4@3	627	5	143	0.007	2.300	3.61	0.212	3.58	1167.7	8.6	1212.2	25.9	1237.3	40.4
NW-4@4	228	1	49	0.005	2.152	3.63	0.200	3.58	1150.3	12.1	1165.8	25.5	1174.1	38.6
NW-4@5	813	5	193	0.007	2.365	3.60	0.220	3.58	1149.8	6.3	1232.1	26.0	1279.7	41.7
NW-4@6	675	10	152	0.015	2.241	3.60	0.208	3.58	1151.7	8.0	1194.0	25.6	1217.4	39.9
NW-4@7	2009	27	470	0.014	2.327	3.69	0.216	3.68	1152.3	6.2	1220.4	26.6	1259.3	42.2
NW-4@8	1137	14	266	0.013	2.341	3.60	0.216	3.58	1162.5	7.0	1224.8	25.9	1260.5	41.1
NW-4@9	851	10	181	0.012	2.126	3.61	0.197	3.58	1153.2	7.8	1157.1	25.2	1159.2	38.1
NW-4@10	2349	22	505	0.010	2.148	3.60	0.199	3.59	1154.2	5.3	1164.4	25.2	1170.0	38.5
NW-4@11	1577	14	364	0.009	2.301	3.59	0.213	3.58	1153.0	4.4	1212.6	25.7	1246.3	40.7
NW-4@12	677	6	158	0.009	2.325	3.60	0.216	3.58	1151.5	6.9	1220.1	25.9	1259.2	41.1
NW-4@13	1183	10	288	0.009	2.443	3.59	0.225	3.58	1163.1	5.1	1255.5	26.2	1310.0	42.6
NW-4@14	1452	12	336	0.009	2.308	3.59	0.214	3.58	1152.8	5.4	1214.7	25.8	1249.8	40.8
NW-4@15	1016	13	242	0.013	2.376	3.61	0.220	3.59	1157.7	8.4	1235.3	26.1	1280.2	41.8
NW-4@16	844	11	195	0.014	2.310	3.60	0.214	3.58	1158.7	7.8	1215.4	25.9	1247.6	40.8
NW-4@17	2229	26	543	0.012	2.425	3.59	0.225	3.58	1149.7	3.8	1250.1	26.1	1309.1	42.6
NW-4@18	1779	31	418	0.018	2.354	3.59	0.217	3.58	1164.3	4.7	1228.8	25.9	1265.9	41.3
NW-4@19	1384	32	317	0.023	2.286	3.59	0.211	3.58	1158.9	4.8	1208.0	25.7	1235.7	40.4
NW-4@20	927	11	204	0.011	2.202	3.59	0.204	3.58	1157.6	5.8	1181.8	25.4	1195.1	39.2
NW-4@21	959	13	223	0.014	2.329	3.60	0.215	3.58	1163.9	6.5	1221.1	25.9	1253.7	40.9
NW-4@22	1326	12	319	0.009	2.417	3.60	0.222	3.58	1167.5	6.7	1247.8	26.2	1294.8	42.2
NW-4@23	1055	11	243	0.011	2.314	3.60	0.213	3.58	1165.4	6.7	1216.7	25.8	1245.8	40.7
NW-4@24	1027	12	241	0.012	2.335	3.60	0.217	3.58	1150.1	6.4	1222.9	25.9	1264.6	41.3
NW-4@25	2400	46	553	0.019	2.299	3.59	0.213	3.58	1158.5	4.0	1212.0	25.7	1242.3	40.6
P10A@1	760	11	163	0.014	2.143	3.46	0.197	3.44	1164.7	7.5	1162.6	24.2	1161.5	36.7
P10A@2	1158	13	260	0.011	2.264	3.46	0.207	3.44	1179.7	8.4	1201.1	24.7	1213.1	38.1
P10A@3	1085	13	237	0.012	2.172	3.46	0.202	3.44	1146.6	8.3	1172.0	24.4	1185.7	37.4
P10A@4	220	2	48	0.011	2.188	3.58	0.200	3.44	1175.8	19.4	1177.1	25.3	1177.9	37.2
P10A@5	832	12	189	0.014	2.266	3.46	0.210	3.44	1152.5	7.8	1201.9	24.7	1229.6	38.6
P10A@6	666	6	133	0.009	1.999	3.48	0.185	3.45	1154.1	9.3	1115.2	23.9	1095.3	34.9
P10A@7	730	14	164	0.019	2.262	3.46	0.207	3.44	1178.5	8.2	1200.7	24.7	1213.0	38.1
P10A@8	759	12	176	0.015	2.331	3.46	0.215	3.44	1166.1	7.1	1221.8	24.9	1253.5	39.4
P10A@9	889	10	193	0.011	2.177	3.46	0.200	3.44	1167.0	6.9	1173.7	24.3	1177.4	37.1
P10A@10	1008	19	232	0.019	2.284	3.46	0.213	3.44	1140.9	7.7	1207.3	24.7	1244.8	39.0
P10A@11	675	8	146	0.012	2.164	3.46	0.199	3.44	1167.2	7.7	1169.6	24.3	1170.9	36.9
P10A@12	827	12	178	0.014	2.148	3.46	0.198	3.44	1159.4	7.6	1164.5	24.3	1167.2	36.8
P10A@13	1287	18	295	0.014	2.298	3.45	0.212	3.44	1161.7	5.6	1211.6	24.7	1239.8	38.9
P10A@14	654	9	139	0.014	2.136	3.47	0.196	3.45	1175.2	8.1	1160.4	24.3	1152.5	36.5
P10A@15	1183	15	255	0.013	2.150	3.45	0.199	3.44	1155.4	6.4	1165.2	24.2	1170.4	36.9
P10A@16	862	9	186	0.011	2.156	3.46	0.199	3.44	1159.1	7.2	1167.0	24.3	1171.2	36.9
P10A@17	318	4	73	0.013	2.309	3.50	0.213	3.44	1158.5	13.0	1215.0	25.1	1247.0	39.1
P10A@18	465	6	103	0.014	2.207	3.50	0.205	3.45	1151.0	10.8	1183.1	24.7	1200.8	38.0
P10A@19	640	9	144	0.014	2.271	3.47	0.207	3.44	1182.3	8.0	1203.4	24.7	1215.2	38.2
P10A@20	685	8	159	0.012	2.326	3.48	0.215	3.44	1158.7	10.4	1220.1	25.0	1255.2	39.3
P10A@21	450	8	96	0.017	2.129	3.49	0.197	3.44	1156.4	12.1	1158.3	24.4	1159.3	36.6
P10A@22	217	2	48	0.011	2.220	3.53	0.204	3.45	1167.0	15.2	1187.2	25.0	1198.4	37.8
P10A@23	487	4	97	0.008	2.009	3.47	0.184	3.44	1180.3	9.4	1118.7	23.8	1087.2	34.5
P10A@24	1067	17	231	0.015	2.166	3.46	0.200	3.44	1164.6	6.2	1170.2	24.3	1173.3	37.0
P10A@25	548	6	118	0.011	2.178	3.47	0.199	3.44	1179.0	8.8	1174.0	24.4	1171.3	37.0
P10A@26	891	13	190	0.015	2.136	3.49	0.197	3.44	1164.3	12.0	1160.6	24.5	1158.6	36.6
P10A@27	1002	16	236	0.016	2.336	3.60	0.217	3.56	1146.0	10.5	1223.3	25.9	1267.6	41.1
P10A@28	591	9	126	0.015	2.141	3.51	0.197	3.44	1170.3	13.0	1162.1	24.6	1157.6	36.6
P10A@29	999	20	229	0.020	2.285	3.46	0.211	3.44	1159.7	7.0	1207.5	24.7	1234.4	38.7
P10A@30	1020	14	229	0.014	2.244	3.46	0.207	3.44	1158.6	6.9	1194.8	24.6	1214.9	38.2
P10A@31	840	23	196	0.028	2.342	3.48	0.215	3.44	1171.1	10.0	1225.1	25.0	1256.0	39.4
P10A@32	710	12	160	0.017	2.263	3.46	0.208	3.44	1168.9	7.6	1200.8	24.7	1218.6	38.3
P10A@33	225	2	53	0.010	2.356	3.52	0.217	3.44	1168.7	14.2	1229.4	25.4	1264.3	39.6
P10A@34	178	1	39	0.008	2.250	3.54	0.205	3.44	1191.5	16.4	1196.7	25.2	1199.6	37.7
P10A@35	2210	41	483	0.019	2.169	3.46	0.202	3.44	1144.0	7.0	1171.0	24.3	1185.7	37.4
~~MT25@1~~	~~1~~	~~0~~	~~[0]~~	~~0.320~~	~~1.303~~	~~35.86~~	~~0.176~~	~~4.63~~	~~353.2~~	~~650.2~~	~~847.2~~	~~230.2~~	~~1047.5~~	~~44.9~~
~~MT25@2~~	~~1~~	~~0~~	~~0~~	~~0.277~~	~~1.784~~	~~8.93~~	~~0.181~~	~~3.48~~	~~975.9~~	~~159.1~~	~~1039.7~~	~~59.8~~	~~1070.3~~	~~34.4~~
MT25@3	5	1	1	0.206	1.997	4.94	0.195	3.07	1051.8	75.9	1114.5	34.0	1147.0	32.4
MT25@4	4	1	1	0.331	2.201	5.82	0.207	3.10	1120.7	95.3	1181.4	41.5	1214.8	34.4
MT25@5	3	1	1	0.289	2.165	6.00	0.188	3.13	1282.1	96.5	1169.7	42.5	1110.0	32.0
MT25@6	5	2	1	0.337	2.017	4.96	0.185	3.08	1172.4	75.2	1121.1	34.3	1094.8	31.1
MT25@7	4	1	1	0.308	2.883	6.99	0.261	3.04	1197.3	119.4	1377.4	54.2	1496.5	40.8
~~MT25@8~~	~~4~~	~~2~~	~~1~~	~~0.520~~	~~1.507~~	~~101.03~~	~~0.191~~	~~6.60~~	~~505.1~~	~~1377.5~~	~~933.0~~	~~481.8~~	~~1124.2~~	~~68.4~~
MT25@9	99	10	18	0.097	1.870	5.82	0.170	3.97	1188.2	81.8	1070.4	39.2	1013.5	37.3
~~MT25@10~~	~~0~~	~~0~~	~~0~~	~~1.135~~	~~1.250~~	~~40.65~~	~~0.171~~	~~3.31~~	~~323.7~~	~~726.1~~	~~823.3~~	~~259.9~~	~~1019.9~~	~~31.3~~
MT25@11	2	2	0	0.873	1.921	8.24	0.176	3.09	1182.3	144.1	1088.6	56.6	1042.4	29.8
~~MT25@12~~	~~1~~	~~1~~	~~0~~	~~1.033~~	~~1.441~~	~~51.35~~	~~0.217~~	~~3.14~~	~~110.9~~	~~901.9~~	~~906.3~~	~~366.7~~	~~1264.5~~	~~36.2~~

https://doi.org/10.1017/S0016756815001120 Published online by Cambridge University Press

Table 1. Continued

Sample/ spot no.	[U] ppm	[Th] ppm	[Pb] ppm	Th/U meas.	$^{207}Pb/^{235}U$	±σ %	$^{206}Pb/^{238}U$	±σ %	$^{207}Pb–^{206}Pb$	±σ	$^{207}Pb–^{235}U$	±σ	$^{206}Pb–^{238}U$	±σ
MT25@13	130	10	28	0.075	2.147	3.37	0.197	3.13	1173.0	24.7	1164.2	23.6	1159.5	33.3
MT25@14	76	6	17	0.073	2.255	3.16	0.206	3.03	1179.1	17.1	1198.3	22.4	1209.0	33.5
~~MT25@15~~	~~1~~	~~0~~	~~0~~	~~0.216~~	~~1.977~~	~~8.22~~	~~0.168~~	~~3.14~~	~~1321.2~~	~~140.6~~	~~1107.7~~	~~57.0~~	~~1002.2~~	~~29.2~~
MT25@16	3	1	1	0.320	1.952	5.55	0.186	3.27	1094.6	87.2	1099.0	38.0	1101.2	33.2
MT25@17	62	18	16	0.297	2.404	3.16	0.218	3.03	1194.3	17.4	1243.7	22.9	1272.3	35.1
~~MT25@18~~	~~2~~	~~0~~	~~0~~	~~0.166~~	~~1.957~~	~~6.79~~	~~0.176~~	~~3.10~~	~~1211.3~~	~~114.4~~	~~1100.7~~	~~46.7~~	~~1045.6~~	~~30.0~~
MT25@19	6	1	1	0.250	2.005	4.44	0.184	3.16	1174.8	60.5	1117.1	30.5	1087.7	31.7
MT25@20	68	6	15	0.093	2.116	3.26	0.200	3.03	1113.0	23.7	1154.2	22.7	1176.3	32.7
P10L@1	302	7	66	0.023	2.219	3.49	0.203	3.44	1182.7	11.5	1187.0	24.7	1189.4	37.5
P10L@2	163	3	36	0.019	2.195	3.53	0.201	3.44	1173.7	16.0	1179.6	24.9	1182.7	37.3
P10L@3	647	16	146	0.025	2.246	3.47	0.208	3.44	1155.2	8.8	1195.7	24.7	1218.1	38.3
P10L@4	306	8	71	0.025	2.294	3.49	0.212	3.44	1158.9	11.5	1210.4	25.0	1239.4	38.9
P10L@5	1959	21	466	0.011	2.369	3.46	0.220	3.44	1150.0	7.2	1233.3	25.0	1281.5	40.1
P10L@6	402	9	95	0.023	2.324	3.49	0.217	3.44	1139.6	11.0	1219.7	25.0	1265.5	39.7
P10L@7	377	10	87	0.026	2.315	3.49	0.213	3.44	1167.1	12.0	1216.8	25.1	1245.0	39.0
P10L@8	400	10	92	0.026	2.278	3.47	0.211	3.44	1155.5	9.8	1205.5	24.8	1233.7	38.7
P10L@9	317	9	71	0.029	2.241	3.52	0.206	3.44	1171.5	14.5	1194.0	25.0	1206.5	38.0
P10L@10	1231	15	272	0.012	2.218	3.47	0.204	3.45	1167.7	7.9	1186.8	24.6	1197.3	37.8
P10L@11	2049	94	495	0.046	2.395	3.45	0.221	3.44	1161.4	5.1	1241.2	25.0	1287.7	40.3
P10L@12	643	13	155	0.020	2.407	3.48	0.222	3.44	1165.2	10.3	1244.8	25.3	1291.3	40.4
P10L@13	824	25	187	0.030	2.263	3.47	0.209	3.45	1160.6	6.7	1200.9	24.7	1223.4	38.6
P10L@14	125	5	27	0.037	2.122	3.57	0.196	3.44	1157.4	18.6	1156.1	24.9	1155.4	36.5
P10L@15	277	6	64	0.023	2.309	3.49	0.214	3.44	1151.0	12.0	1215.2	25.0	1251.7	39.2
P10L@16	189	6	43	0.031	2.239	3.53	0.207	3.44	1157.6	15.5	1193.5	25.1	1213.4	38.1
P10L@17	830	10	191	0.012	2.297	3.49	0.212	3.45	1159.7	10.4	1211.5	25.0	1240.7	39.0
P10L@18	571	21	128	0.037	2.221	3.47	0.206	3.44	1151.0	8.6	1187.5	24.6	1207.7	38.0
P10L@19	266	5	58	0.019	2.165	3.56	0.200	3.44	1157.1	17.8	1169.9	25.0	1176.8	37.1
P10L@20	1583	16	388	0.010	2.438	3.45	0.227	3.44	1144.4	5.7	1253.9	25.1	1318.7	41.1
P10L@21	288	7	66	0.023	2.311	3.60	0.211	3.46	1180.2	19.8	1215.6	25.9	1235.7	39.0
P10L@22	200	6	47	0.030	2.330	3.51	0.213	3.44	1180.6	14.0	1221.4	25.3	1244.6	39.0
P10L@23	405	9	89	0.023	2.208	3.48	0.203	3.44	1171.3	11.1	1183.6	24.6	1190.4	37.5
P10L@24	214	9	48	0.041	2.243	3.51	0.206	3.44	1174.0	13.4	1194.7	24.9	1206.2	37.9
P10L@25	458	13	114	0.029	2.471	3.50	0.229	3.47	1157.6	9.7	1263.5	25.6	1326.7	41.7
P10L@26	269	8	61	0.030	2.238	3.51	0.208	3.44	1145.5	14.2	1193.2	25.0	1219.7	38.3
P10L@27	322	18	74	0.055	2.296	3.49	0.209	3.44	1189.0	11.5	1211.1	25.0	1223.6	38.4
P10L@28	528	12	118	0.023	2.236	3.47	0.206	3.44	1162.4	8.6	1192.3	24.6	1208.9	38.0
P10L@29	356	13	85	0.036	2.392	3.50	0.219	3.44	1176.8	12.4	1240.1	25.3	1276.8	40.0
P10L@30	414	9	91	0.021	2.194	3.56	0.203	3.44	1160.9	18.2	1179.3	25.1	1189.3	37.4
P10L@31	407	22	101	0.054	2.427	3.50	0.226	3.46	1145.3	11.3	1250.6	25.5	1312.6	41.2
P10L@32	520	20	118	0.039	2.226	3.47	0.208	3.44	1141.2	9.1	1189.3	24.6	1216.0	38.2
P10L@33	708	19	161	0.027	2.259	3.47	0.209	3.44	1155.5	9.8	1199.6	24.8	1224.2	38.5
P10L@34	428	19	98	0.045	2.242	3.50	0.209	3.44	1144.2	12.8	1194.4	24.9	1222.3	38.4
P10L@35	526	17	132	0.032	2.513	3.51	0.230	3.44	1178.9	13.1	1275.9	25.8	1334.2	41.6

The crossed data are not included in age calculation owing to their low U and Th abundances, and hence large errors in isotopic ratio.

4.c. Apatite U–Pb age

Apart from baddeleyite, apatites from the carbonatite NW-1 and NW-4 samples were selected for U–Pb analyses by TIMS and *in situ* techniques. Apatite NW-1 is characterized by high U concentrations of 61–168 ppm (with an average value of 115 ppm) constrained by laser ablation analyses (online Supplementary Material available at http://journals.cambridge.org/geo), making it a potential standard for apatite SIMS age determination (Li *et al.* 2012). Ten analyses on this sample by TIMS yielded a $^{206}Pb–^{238}U$ age of 1168.3 ± 4.5 Ma, a $^{207}Pb–^{235}U$ age of 1162.1 ± 3.3 Ma and a $^{207}Pb–^{206}Pb$ age of 1155.3 ± 5.8 Ma, showing a slight discordance (Table 2; Fig. 6a). Using the SIMS technique, the calculated $^{207}Pb–^{206}Pb$ age is 1167 ± 40 Ma (Fig. 6b). Using NW-1 as a calibration standard for the laser ablation analyses, the NW-4 apatite gives an intercept age of 1166 ± 28 Ma on the Tera-Wasserburg diagram (Fig. 6c). If the ^{207}Pb correction method is applied, the obtained weighted mean $^{206}Pb–^{238}U$ age is 1153 ± 24 Ma (Fig. 6c), identical to the ages obtained above from baddeleyite within errors. It is noted that the composition of common lead is critical to calculation of the above ages obtained by both SIMS and laser ablation techniques. In our work, the model of Stacey & Kramers (1975) at 1160 Ma was applied. Fortunately, our apatites have low common lead, and the data cluster proximal to the Concordia curve (Fig. 6). In this case, the calculated age is not significantly controlled by the uncertainty of common lead composition.

4.d. Sr–Nd–Hf isotopic compositions

4.d.1 Apatite

Apatite has been extracted from all the samples investigated, and analysed for its Sr and Nd isotopic compositions using an *in situ* laser ablation technique (Table 3). All of the apatites have low

https://doi.org/10.1017/S0016756815001120 Published online by Cambridge University Press

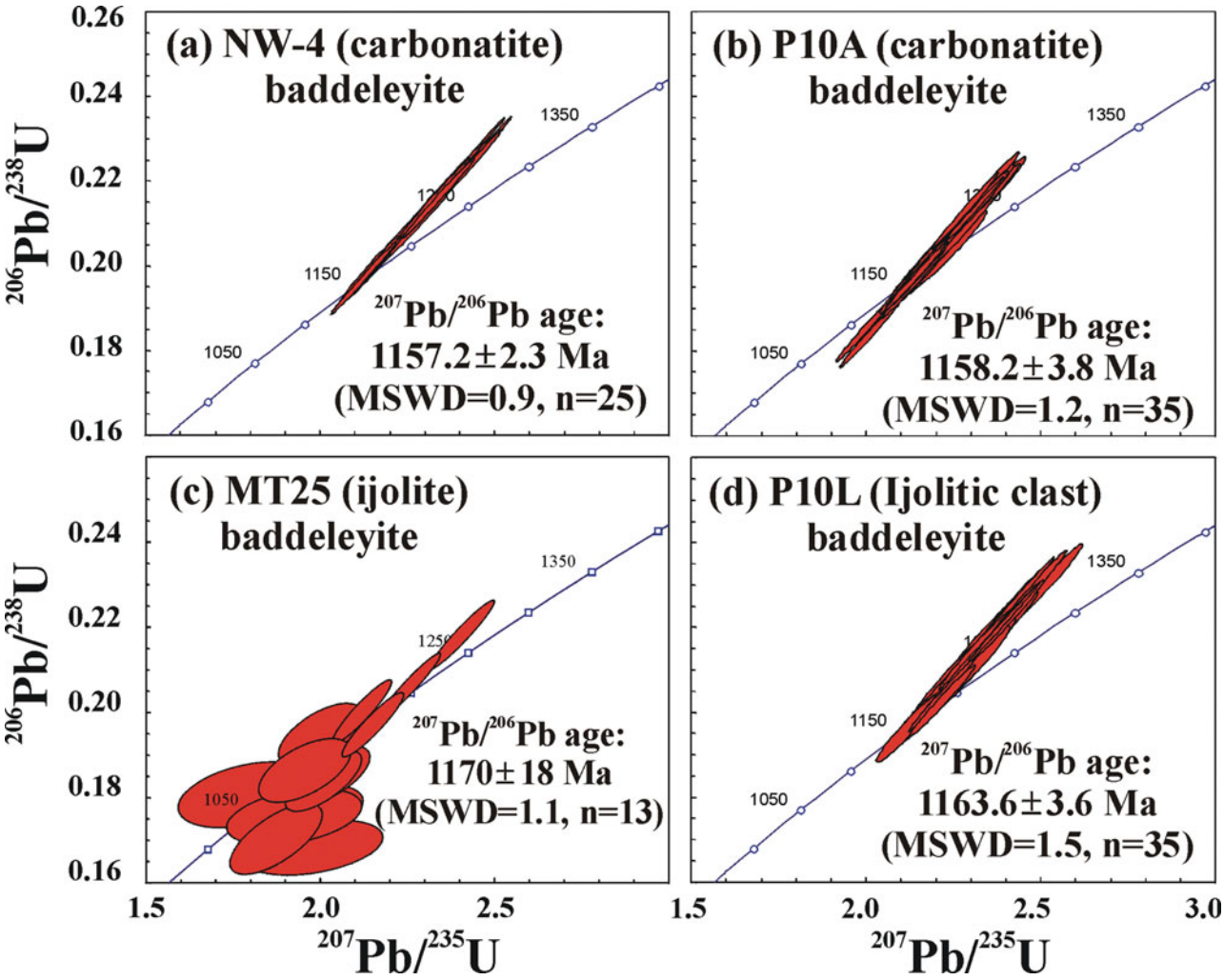

Figure 5. (Colour online) Baddeleyite U–Pb Concordia diagrams for the Prairie Lake complex. (a) NW-4 (carbonatite); (b) P10A (carbonatite); (c) MT25 (ijolite); and (d) P10L (ijolitic clast within carbonatite).

^{87}Rb/^{86}Sr ratios (0.00001–0.00013) with ^{87}Sr/^{86}Sr ratios ranging from 0.70246 ± 3 to 0.70261 ± 2 (Table 3; Fig. 7a). In terms of rock type, ^{87}Rb/^{86}Sr and ^{87}Sr/^{86}Sr ratios are: 0.00002–0.00013 and 0.70251 ± 2 to 0.70261 ± 2 for carbonatite; 0.00001–0.00012 and 0.70246 ± 3 to 0.70260 ± 2 for ijolite; and 0.00001–0.00002 and 0.70253 ± 2 to 0.70260 ± 3 for syenite, respectively. The weighted average ^{87}Sr/^{86}Sr ratios are 0.70251 ± 2 for carbonatite (2σ, n = 8), 0.70253 ± 2 for ijolite (2σ, n = 25) and 0.70256 ± 5 for syenite (2σ, n = 4), respectively (Fig. 7a). These data indicate that there is no significant variation among the different rocks within the complex, and the average value of 0.70253 ± 1 for all samples (2σ, n = 37) can be considered as the best estimation of the initial Sr isotopic composition of apatite for the Prairie Lake complex.

The ^{147}Sm/^{144}Nd ratios and ^{143}Nd/^{144}Nd isotopic compositions of apatite range from 0.0690 to 0.1094 and from 0.511806 ± 51 to 0.512142 ± 10, respectively (Table 3; Fig. 8a). For the individual rocks within the complex, the ^{147}Sm/^{144}Nd and ^{143}Nd/^{144}Nd ratios of the carbonatite range from 0.1006 to 0.1094 and from 0.512080 ± 10 to 0.512142 ± 10, respectively. The calculated $\varepsilon_{Nd}(t)_{1160}$ values are from +3.1 ± 0.2 (PL97) to +3.7 ± 0.1 (NW-1), with an average value of +3.44 ± 0.20 (2σ, n = 8) (Fig. 8a). Apatite from the ijolite shows larger variations of ^{147}Sm/^{144}Nd from 0.0690 to 0.1064 and ^{143}Nd/^{144}Nd from 0.511806 ± 51 to 0.512141 ± 20, with $\varepsilon_{Nd}(t)_{1160}$ values of +2.6 ± 0.5 and +4.1 ± 0.2 and an average value of +3.55 ± 0.17 (2σ, n = 25) (Fig. 8a). For the syenite in the complex, apatites have ^{147}Sm/^{144}Nd values of 0.0738 to 0.0848 and a ^{143}Nd/^{144}Nd ratio of 0.511883 ± 10 to 0.511984 ± 18, with $\varepsilon_{Nd}(t)_{1160}$ values of +3.1 ± 0.3 to +4.0 ± 0.2 and an average value of +3.61 ± 0.49 (2σ, n = 4) (Fig. 8a). Therefore, the $\varepsilon_{Nd}(t)_{1160}$ values of apatite from the carbonatite (+3.44 ± 0.20), ijolite (+3.55 ± 0.17) and syenite (+3.61 ± 0.49) are identical within analytical uncertainties, and the average value of +3.52 ± 0.11 (n = 37) for all the samples represents the best estimate of the $\varepsilon_{Nd}(t)_{1160}$ value for the complex.

In addition, it is noted that the apatite from the gneissic xenolith has a much lower ^{87}Sr/^{86}Sr ratio of 0.70170 ± 11 compared to those from the carbonatite, ijolite and syenite. Its ^{147}Sm/^{144}Nd and ^{143}Nd/^{144}Nd

https://doi.org/10.1017/S0016756815001120 Published online by Cambridge University Press

Table 2. TIMS U–Pb isotopic data of the NW-1 apatite

					Isotopic ratio uncorrected			
Sample	U (ppm)	Pb (ppm)	Th (ppm)	Th/U	$^{206}Pb/^{204}Pb$	$^{238}U/^{206}Pb$	2σ (%)	$^{207}Pb/^{206}Pb$	2σ (%)
NW-1 A	84.6	18.1	33.4	0.39	1131.2	4.9676	0.0522	0.0899	0.5447
NW-1 B	68.1	14.6	27.1	0.40	1067.0	4.9767	0.0470	0.0898	0.9467
~~NW-1 C~~	~~32.5~~	~~9.0~~	27.9	~~0.86~~	~~556.6~~	~~4.3026~~	~~0.0567~~	~~0.1024~~	~~1.8139~~
NW-1 p1	67.9	14.4	24.1	0.35	1289.9	4.9514	0.0529	0.0882	0.6037
NW-1 p2	100.5	21.1	34.1	0.34	1242.3	4.9777	0.0515	0.0889	0.5576
NW-1 p3	74.8	16.0	28.4	0.38	893.9	4.9828	0.0505	0.0924	0.8370
NW-1 p4	100.0	22.4	46.9	0.47	788.2	4.8957	0.0467	0.0950	0.7453
NW-1 07	159.6	32.9	43.7	0.27	1411.0	4.9976	2.1355	0.0881	2.0180
NW-1 08	138.5	29.5	47.1	0.34	967.3	4.9778	0.3512	0.0932	0.3032
NW-1 09	118.1	26.0	45.5	0.39	985.2	4.8702	1.1414	0.0921	1.0482
NW-1 10	120.5	26.1	47.8	0.40	1136.8	4.9428	1.3591	0.0906	1.2856

	Isotopic data (^{204}Pb corrected)					Isotopic age (Ma)			
Sample	$^{207}Pb/^{235}U$	2σ (%)	$^{206}Pb/^{238}U$	2σ (%)	$^{207}Pb/^{206}Pb$	2σ (%)	$^{206}Pb–^{238}U$	$^{207}Pb–^{235}U$	$^{207}Pb–^{206}Pb$
NW-1 A	2.13896	0.085	0.198512	0.052	0.0781	0.063	1167.3 ± 0.6	1161.5 ± 0.6	1150.6 ± 1.3
NW-1 B	2.12966	0.082	0.198115	0.047	0.0780	0.064	1165.2 ± 0.5	1158.5 ± 0.6	1145.9 ± 1.3
~~NW-1 C~~	~~2.49762~~	~~0.120~~	~~0.226265~~	~~0.057~~	~~0.0801~~	~~0.098~~	~~1314.9~~ ± 0.7	~~1271.3~~ ± 0.9	~~1198.4~~ ± 1.9
NW-1 p1	2.14867	0.079	0.199547	0.053	0.0781	0.056	1172.9 ± 0.6	1164.6 ± 0.5	1149.3 ± 1.1
NW-1 p2	2.14333	0.079	0.198378	0.051	0.0784	0.057	1166.6 ± 0.5	1162.9 ± 0.5	1156.0 ± 1.1
NW-1 p3	2.11561	0.088	0.197231	0.050	0.0778	0.068	1160.4 ± 0.5	1153.9 ± 0.6	1141.7 ± 1.3
NW-1 p4	2.15778	0.089	0.200197	0.047	0.0782	0.071	1176.4 ± 0.5	1167.6 ± 0.6	1151.2 ± 1.4
NW-1 07	2.13262	0.147	0.197514	0.134	0.0783	0.055	1162.0 ± 1.4	1159.4 ± 1.0	1154.7 ± 1.1
NW-1 08	2.13657	0.139	0.197024	0.137	0.0786	0.022	1159.3 ± 1.5	1160.7 ± 1.0	1163.3 ± 0.4
NW-1 09	2.16571	0.122	0.201487	0.116	0.0780	0.035	1183.3 ± 1.3	1170.1 ± 0.8	1145.8 ± 0.7
NW-1 10	2.15057	0.146	0.199035	0.116	0.0784	0.082	1170.1 ± 1.2	1165.2 ± 1.0	1156.1 ± 1.6
						Average	**1168.3 ± 4.4**	**1162.1 ± 3.3**	**1155.3 ± 5.8**

Analysed by Kevin R. Chamberlain (University of Wyoming, UWYO), and Yuri Amelin (Australian National University, ANU).
Sample NW-1 C was not included in age calculation owing to its significant discordance.

ratios are 0.0968 and 0.510924 ± 63, respectively, with an $\varepsilon_{Nd}(t)_{1160}$ value of −19.1 ± 0.6 and a depleted mantle model age of 2.88 Ga (Table 3; Fig. 8a), indicating its derivation from the Archaean country rocks.

4.d.2 Calcite

Calcite has low REE contents; thus, only Sr isotopic compositions were determined (Table 3). Comparatively, calcite has even lower $^{87}Rb/^{86}Sr$ ratios than apatite (Fig. 7b). Of the eight samples of calcite extracted from the carbonatite, the $^{87}Rb/^{86}Sr$ and $^{87}Sr/^{86}Sr$ ratios are 0.00000–0.00006 and 0.70250 ± 2 to 0.70261 ± 2 with an average $^{87}Sr/^{86}Sr$ ratio of 0.70253 ± 3 (2σ, n = 8). Of the 23 samples of calcite from the ijolite, their $^{87}Rb/^{86}Sr$ and $^{87}Sr/^{86}Sr$ ratios are 0.00000–0.00008 and 0.70245 ± 4 to 0.70262 ± 2, with an average $^{87}Sr/^{86}Sr$ ratio of 0.70254 ± 2 (2σ, n = 23). The calcite samples from the syenite also have uniform $^{87}Rb/^{86}Sr$ (< 0.00002) and $^{87}Sr/^{86}Sr$ (from 0.70255 ± 3 to 0.70259 ± 1) ratios, with an average $^{87}Sr/^{86}Sr$ ratio of 0.70258 ± 3 (2σ, n = 4). Therefore, calcites from the carbonatite (0.70253 ± 3), ijolite (0.70254 ± 2) and syenite (0.70258 ± 3) have identical Sr isotopic compositions, and an average of 0.70255 ± 1 (2σ, n = 35). These values are comparable to those of apatite from the carbonatite (0.70251 ± 2), ijolite (0.70253 ± 2) and syenite (0.70256 ± 5).

4.d.3 Perovskite

Five perovskite samples from the carbonatite and ijolite were selected for Sr–Nd isotopic analysis (Table 3). Of these samples, only two perovskites (NW-1 and WT8) were adequate for Rb–Sr isotope study, and give $^{87}Rb/^{86}Sr$ ratios of 0.0001 to 0.0038 and $^{87}Sr/^{86}Sr$ ratios of 0.70232 ± 7 to 0.70273 ± 11 (Table 3; Fig. 7c). The weighted $^{87}Sr/^{86}Sr$ ratios are 0.70263 ± 5 (n = 8) for NW-1 and 0.70253 ± 3 (n = 16) for WT8. In terms of Nd isotopic data (Fig. 8b), perovskites from the five samples show similar isotopic variations to those of apatite, with $^{147}Sm/^{144}Nd$, $^{143}Nd/^{144}Nd$ and $\varepsilon_{Nd}(t)_{1160}$ values ranging from 0.0573 to 0.1088, 0.51176 ± 4 to 0.51216 ± 9, and +1.9 ± 1.4 to +4.9 ± 1.0, respectively. Their average $\varepsilon_{Nd}(t)_{1160}$ value is +3.37 ± 0.14 (n = 66), comparable to that of apatite.

4.d.4 Titanite

Titanite was extracted only from four samples and only Sm–Nd isotopic data were obtained. The $^{147}Sm/^{144}Nd$ and $^{143}Nd/^{144}Nd$ isotopic ratios range from 0.1084 to 0.1475, and 0.512139 ± 24 to 0.512448 ± 45, respectively, with $\varepsilon_{Nd}(t)_{1160}$ values from +3.3 ± 0.4 to +3.5 ± 0.3 (Table 3; Figs 8c). The calculated average $\varepsilon_{Nd}(t)_{1160}$ value is +3.39 ± 0.15 (n = 62), identical to that of apatite and perovskite.

https://doi.org/10.1017/S0016756815001120 Published online by Cambridge University Press

Table 3. Sr–Nd isotopic data of minerals from the Prairie Lake complex

Sample	Lithology	Mineral	$^{87}Rb/^{86}Sr$	$^{87}Sr/^{86}Sr$	2σ	I_{Sr}	$^{147}Sm/^{144}Nd$	$^{143}Nd/^{144}Nd$	2σ	T_{DM}	$\varepsilon_{Nd}(t)$	2σ	$f_{Sm/Nd}$
NW-1	Carbonatite	Ap	0.000054	0.702507	13	0.7025	0.1022	0.512108	7	1422	3.74	0.14	−0.48
NW-1	Carbonatite	Cc	0.000001	0.702510	14	0.7025							
NW-1	Carbonatite	Prv	0.000118	0.702628	54	0.7026	0.0783	0.511890	13	1416	3.07	0.31	−0.60
NW-4	Carbonatite	Ap	0.000056	0.702488	12	0.7025	0.1067	0.512141	9	1435	3.68	0.17	−0.46
NW-4	Carbonatite	Cc	0.000020	0.702495	17	0.7025							
S-2	Carbonatite	Ap	0.000025	0.702519	21	0.7025	0.1006	0.512080	10	1440	3.38	0.20	−0.49
S-2	Carbonatite	Cc	0.000007	0.702537	18	0.7025							
P10A	Carbonatite	Ap	0.000075	0.702522	14	0.7025	0.1064	0.512125	8	1453	3.41	0.22	−0.46
P10A	Carbonatite	Cc	0.000058	0.702538	14	0.7025							
P10B	Carbonatite	Ap	0.000127	0.702612	22	0.7026	0.1094	0.512142	10	1470	3.30	0.20	−0.44
P10B	Carbonatite	Cc	0.000009	0.702610	19	0.7026							
P10E	Carbonatite	Ap	0.000017	0.702523	18	0.7025	0.1021	0.512095	9	1439	3.47	0.18	−0.48
P10E	Carbonatite	Cc	0.000007	0.702524	19	0.7025							
PL97	Carbonatite	Ap	0.000037	0.702546	16	0.7025	0.1048	0.512093	11	1477	3.06	0.22	−0.47
PL97	Carbonatite	Cc	0.000036	0.702573	23	0.7026							
PL110	Carbonatite	Ap	0.000073	0.702505	16	0.7025	0.1061	0.512113	7	1467	3.23	0.14	−0.46
PL110	Carbonatite	Cc	0.000000	0.702522	19	0.7025							
P10L	Mafic clast	Ap	0.000020	0.702514	17	0.7025	0.1052	0.512094	11	1482	2.98	0.22	−0.46
P10L	Mafic clast	Cc	0.000020	0.702535	12	0.7025							
MT04/05-1	Ijolite	Ap	0.000115	0.702542	39	0.7025	0.0965	0.512058	7	1418	3.59	0.18	−0.51
MT04/05-1	Ijolite	Cc	0.000004	0.702549	31	0.7025							
MT04/05-2	Ijolite	Ap	0.000053	0.702515	35	0.7025	0.0984	0.512058	9	1441	3.31	0.24	−0.50
MT04/05-2	Ijolite	Cc	0.000003	0.702614	57	0.7026							
MT04/06	Ijolite	Ap	0.000022	0.702515	19	0.7025	0.0847	0.511943	14	1424	3.14	0.16	−0.57
MT04/06	Ijolite	Cc	0.000002	0.702621	15	0.7026							
MT04/10-1	Ijolite	Ap	0.000024	0.702554	30	0.7026	0.0796	0.511939	22	1375	3.94	0.39	−0.60
MT04/10-1	Ijolite	Cc	0.000060	0.702536	42	0.7025							
MT04/15-1	Ijolite	Ap	0.000018	0.702586	30	0.7026	0.0865	0.512001	22	1375	3.74	0.27	−0.56
MT04/15-1	Ijolite	Cc	0.000000	0.702549	25	0.7025							
MT09/10	Ijolite	Ap	0.000028	0.702547	29	0.7025	0.0690	0.511873	30	1343	3.77	0.23	−0.65
MT09/10	Ijolite	Cc	0.000000	0.702552	30	0.7026							
MT24	Ijolite	Ap	0.000050	0.702548	25	0.7025	0.0944	0.512044	13	1411	3.74	0.15	−0.52
MT25	Ijolite	Ap	0.000009	0.702508	39	0.7025	0.1049	0.512141	20	1411	3.95	0.37	−0.47
MT25	Ijolite	Cc	0.000025	0.702512	36	0.7025							
MT26	Ijolite	Ap	0.000009	0.702548	14	0.7025	0.0777	0.511934	34	1361	4.09	0.22	−0.60
MT26	Ijolite	Cc	0.000002	0.702590	15	0.7026							
NE2	Ijolite	Ap	0.000015	0.702503	28	0.7025	0.0793	0.511806	51	1521	2.60	0.46	−0.60
NE2	Ijolite	Cc	0.000002	0.702499	29	0.7025							
NE3-1	Ijolite	Ap	0.000026	0.702481	26	0.7025	0.0850	0.511960	35	1407	3.66	0.29	−0.57
NE3-1	Ijolite	Cc	0.000006	0.702493	27	0.7025							
NE3-1	Ijolite	Prv					0.0974	0.512602	34	719	3.58	0.47	−0.50
NE4-1	Ijolite	Ap	0.000006	0.702603	24	0.7026	0.0759	0.511940	28	1337	3.71	0.19	−0.61
NE4-1	Ijolite	Cc	0.000005	0.702528	23	0.7025							
NE5-1	Ijolite	Prv					0.0972	0.511975	67	1534	3.54	0.23	−0.51
NE5-1	Ijolite	Ap	0.000050	0.702479	40	0.7025	0.0769	0.511870	11	1424	2.93	0.25	−0.61
NE5-1	Ijolite	Cc	0.000000	0.702540	32	0.7025							
NE5-2	Ijolite	Ap	0.000036	0.702464	33	0.7025	0.0714	0.511846	10	1395	3.10	0.18	−0.64
NE5-2	Ijolite	Cc	0.000000	0.702536	27	0.7025							
NW5	Ijolite	Ap	0.000044	0.702462	25	0.7025	0.0897	0.511935	66	1491	2.76	0.45	−0.54
NW5	Ijolite	Tit					0.1277	0.512249	32	1594	3.31	0.30	−0.35
NW5	Ijolite	Cc	0.000001	0.702536	32	0.7025							
WS20	Ijolite	Ap	0.000016	0.702595	19	0.7026	0.0881	0.512015	15	1376	3.99	0.26	−0.55
WT1	Ijolite	Ap	0.000031	0.702490	61	0.7025	0.1064	0.512129	18	1448	3.69	0.37	−0.46
WT1	Ijolite	Cc	0.000081	0.702448	38	0.7024							
WT2	Ijolite	Prv	0.002000	0.702710	960	0.7027	0.1000	0.512010	100	1525	3.32	0.44	−0.49
WT2	Ijolite	Ap	0.000036	0.702500	42	0.7025	0.0955	0.512043	26	1425	3.65	0.46	−0.51
WT2	Ijolite	Cc	0.000004	0.702498	49	0.7025							
WT3	Ijolite	Ap	0.000052	0.702513	27	0.7025	0.0969	0.512082	19	1392	4.02	0.38	−0.51
WT3	Ijolite	Tit					0.1420	0.512402	29	1587	3.48	0.26	−0.28
WT3	Ijolite	Cc	0.000002	0.702523	27	0.7025							
WT4	Ijolite	Ap	0.000020	0.702543	25	0.7025	0.0860	0.511979	58	1396	3.92	0.18	−0.56
WT4	Ijolite	Tit					0.1084	0.512139	24	1461	3.26	0.38	−0.45
WT4	Ijolite	Cc	0.000000	0.702593	17	0.7026							
WT5	Ijolite	Ap	0.000021	0.702531	26	0.7025	0.0902	0.512019	32	1394	3.72	0.42	−0.54
WT5	Ijolite	Cc	0.000001	0.702542	20	0.7025							
WT6	Ijolite	Ap	0.000010	0.702478	37	0.7025	0.0840	0.511927	26	1435	2.84	0.37	−0.57
WT6	Ijolite	Cc	0.000000	0.702484	39	0.7025							
WT7	Ijolite	Ap	0.000019	0.702540	31	0.7025	0.0959	0.512004	35	1480	2.66	0.72	−0.51
WT7	Ijolite	Tit					0.1475	0.512448	45	1613	3.44	0.30	−0.25
WT7	Ijolite	Cc	0.000009	0.702506	43	0.7025							
WT8	Ijolite	Prv	0.000260	0.702528	33	0.7025	0.0932	0.512029	32	1416	3.33	0.34	−0.53
WT8	Ijolite	Ap	0.000041	0.702485	35	0.7025	0.0911	0.512050	19	1366	4.08	0.28	−0.54
WT8	Ijolite	Cc	0.000001	0.702481	59	0.7025							

https://doi.org/10.1017/S0016756815001120 Published online by Cambridge University Press

Table 3. Continued

Sample	Lithology	Mineral	$^{87}Rb/^{86}Sr$	$^{87}Sr/^{86}Sr$	2σ	I_{Sr}	$^{147}Sm/^{144}Nd$	$^{143}Nd/^{144}Nd$	2σ	T_{DM}	$\varepsilon_{Nd}(t)$	2σ	$f_{Sm/Nd}$
HGZ2	Ne syenite	Ap	0.000013	0.702586	15	0.7026	0.0738	0.511883	10	1379	3.61	0.20	– 0.62
HGZ2	Ne syenite	Cc	0.000008	0.702572	29	0.7026							
MT04/16	Ne syenite	Ap	0.000020	0.702547	24	0.7025	0.0848	0.511984	18	1377	3.98	0.21	– 0.57
MT04/16	Ne syenite	Cc	0.000004	0.702556	30	0.7026							
Ws2c	Woll syenite	Ap	0.000021	0.702595	25	0.7026	0.0762	0.511886	18	1399	3.10	0.31	– 0.61
Ws2c	Woll syenite	Cc	0.000004	0.702591	9	0.7026							
HGZ3	Woll syenite	Ap	0.000014	0.702531	15	0.7025	0.0747	0.511887	10	1383	3.49	0.19	– 0.62
HGZ3	Woll syenite	Cc	0.000003	0.702553	16	0.7026							
X1	Xenolith	Ap	0.000103	0.701700	110	0.7017	0.0968	0.510924	63	2884	– 19.11	0.64	– 0.51

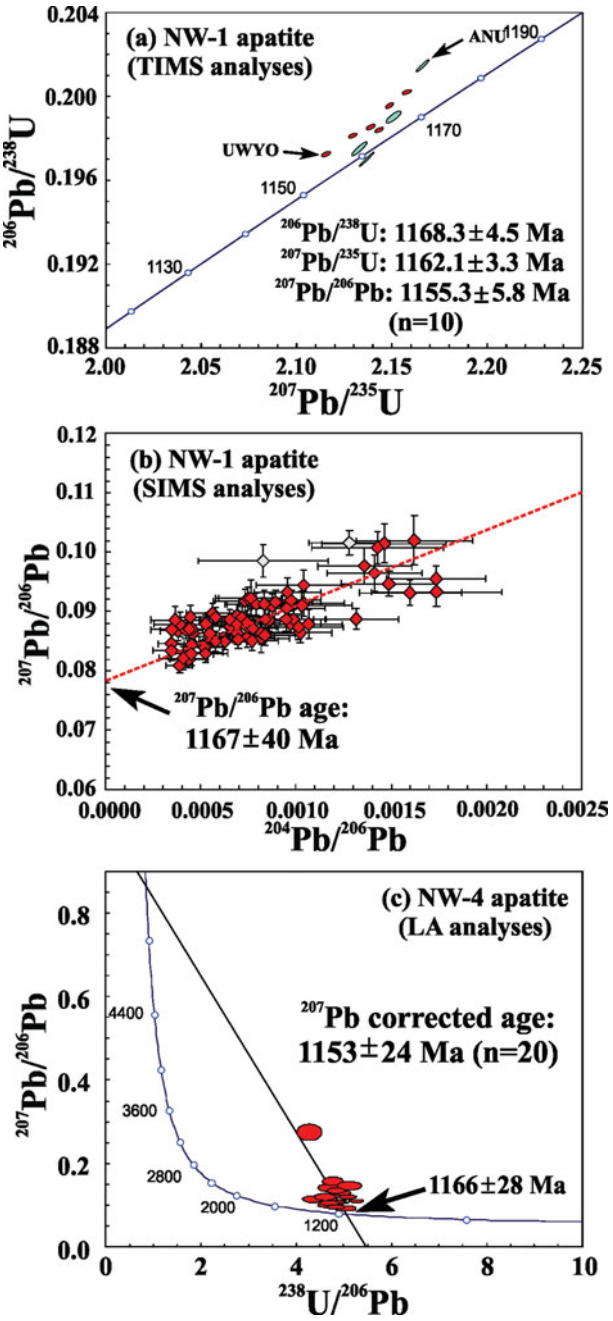

Figure 6. (Colour online) U–Pb diagrams for apatite from the Prairie Lake complex. (a) NW-1 (carbonatite, TIMS data); (b) NW-1 (carbonatite, SIMS data, the plots in grey are excluded for age calculation); (c) NW-4 (carbonatite, laser ablation data).

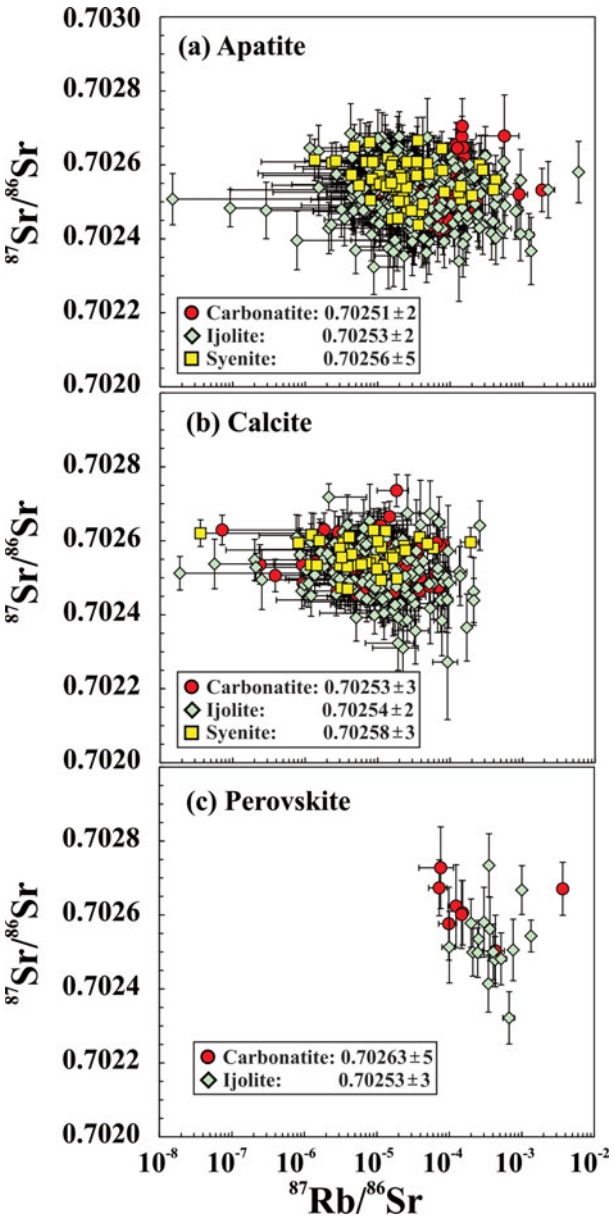

Figure 7. (Colour online) Sr isotopic variations of (a) apatite, (b) calcite and (c) perovskite.

4.d.5 Baddeleyite

Six samples of baddeleyite from the carbonatite and ijolite were analysed for Hf isotopic compositions (Table 4). All have $^{176}Lu/^{177}Hf$ ratios less

https://doi.org/10.1017/S0016756815001120 Published online by Cambridge University Press

Table 4. Lu–Hf isotopic data of baddeleyite from the Prairie Lake complex

Sample	Lithology	$^{176}Lu/^{177}Hf$	$^{176}Hf/^{177}Hf$	2σ	$\varepsilon_{Hf}(t)$	2σ	T_{DM1}	T_{DM2}	$f_{Lu/Hf}$
NW-4	Carbonatite	0.000634	0.282207	13	5.25	0.46	1459	689	– 0.98
P10A	Carbonatite	0.000502	0.282178	9	4.32	0.32	1494	764	– 0.98
PL97	Carbonatite	0.000224	0.282173	8	4.36	0.28	1490	746	– 0.99
PL110	Carbonatite	0.000990	0.282205	19	4.90	0.67	1476	739	– 0.97
P10L	Ijolitic clast	0.000584	0.282193	16	4.79	0.57	1477	727	– 0.98
MT25	Ijolite	0.000132	0.282180	22	4.68	0.78	1477	712	– 1.00

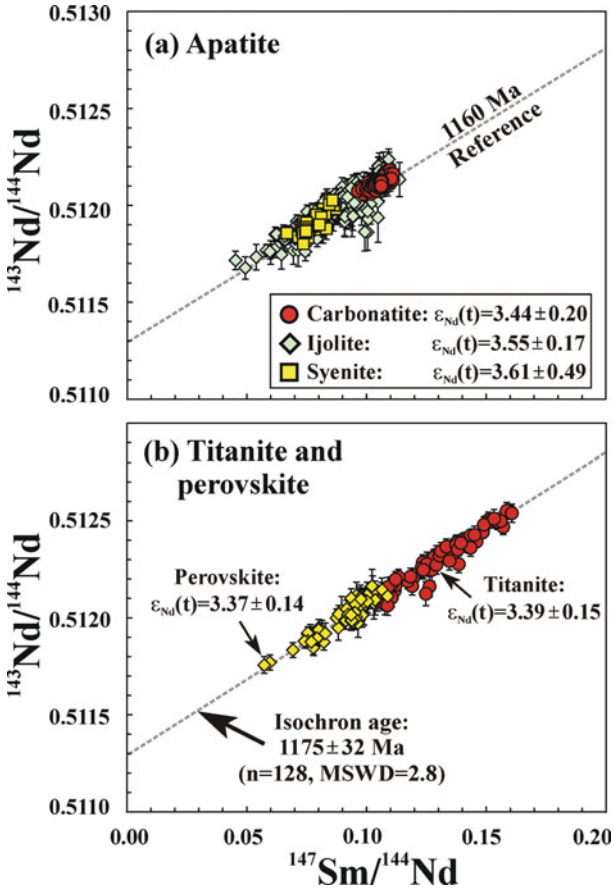

Figure 8. (Colour online) Nd isotopic variations of (a) apatite and (b) titanite and perovskite.

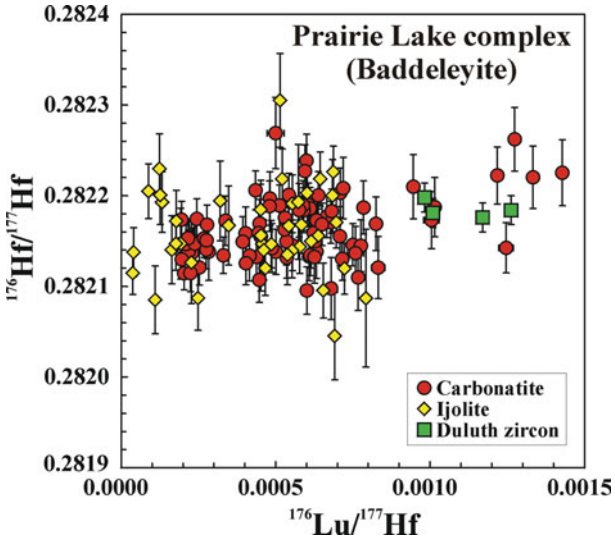

Figure 9. (Colour online) Hf isotopic variations of baddeleyite. Data for the Duluth zircon are from Woodhead & Hergt (2005), Kemp *et al.* (2009), Kimura, Tani & Chang (2012) and Fisher, Vervoort & Dufrane (2014).

than 0.0008, except those of P97, which have much higher $^{176}Lu/^{177}Hf$ ratios (Fig. 9). The average $^{176}Lu/^{177}Hf$, $^{176}Hf/^{177}Hf$ and $\varepsilon_{Hf}(t)_{1160}$ values are from 0.0002 to 0.0010, 0.282173 ± 8 to 0.282207 ± 13, and +4.32 ± 0.32 to +5.25 ± 0.46, respectively (Table 4), with an average $\varepsilon_{Hf}(t)_{1160}$ value of +4.56 ± 0.47 (n = 6). However, if the data are separated according to rock type, the carbonatite and ijolite have $\varepsilon_{Hf}(t)_{1160}$ values of +4.53 ± 0.64 (n = 4) and +4.79 ± 0.57 (n = 2), consistent within uncertainties.

5. Discussion

5.a. Emplacement age of the Prairie Lake complex

The Prairie Lake complex intruded Archaean granitic gneisses, and is considered to have been emplaced during the Proterozoic Era. The first ages of 1164 and 1059 Ma were determined for biotite in the carbonatite by the K–Ar method (Gittins, Macintyre & York, 1967). Subsequently, isochron ages of 1030 ± 60 Ma (Bottrell, 1975), 1033 ± 59 Ma (Bell & Blenkinsop, 1980) and 1030 ± 70 Ma (Bell *et al.* 1982) were determined by Rb–Sr methods. In a subsequent study, S. J. Pollock (unpub. MSc thesis, Carleton Univ., 1987) obtained ages of 1165 ± 30 Ma (Rb–Sr isochron for whole-rock ijolite–carbonatite), 1135 ± 15 Ma (Rb–Sr isochron of biotite), 1130 ± 10 Ma (Rb–Sr isochron of whole-rock ijolite–carbonatite and biotite) and 1200 ± 40 Ma (Sm–Nd isochron of whole-rock ijolite–carbonatite plus separated apatite, calcite and garnet). Given the potential late-stage hydrothermal alteration, these authors suggested that the age of 1165 ± 30 Ma could be the best estimate for the emplacement time of the complex. Bell & Blenkinsop (1989) reported a whole-rock Rb–Sr age of 1023 ± 74 Ma for the carbonatites, and Kwon, Tilton & Grüenenfelder (1989) reported a Pb–Pb age of 1155 ± 36 Ma for calcite in the carbonatite. Note that the isochron ages have very large errors, and mineral ages are required to constrain the emplacement time of the complex.

Using the SIMS technique, Sano *et al.* (1999) obtained a U–Pb age with a large error of 1156 ± 45 Ma for apatite from ijolite. Recently, Rukhlov & Bell

https://doi.org/10.1017/S0016756815001120 Published online by Cambridge University Press

(2010) using TIMS analysis for baddeleyite and zircon from phoscorite, obtained an age of 1164 ± 4 Ma. Similarly, Wu *et al.* (2010) reported a Pb–Pb age of 1159 ± 5 Ma for calzirtite from the carbonatite. These data indicate that the complex was most probably emplaced at ~1160 Ma. Nevertheless, it remained unclear as to whether the different rocks of the complex were emplaced synchronously since these ages were obtained from different laboratories using different methods.

In this study, two samples of baddeleyite from the carbonatite gave ^{207}Pb–^{206}Pb ages of 1157 ± 2 (NW-4) and 1158 ± 4 (P10A) Ma. A TIMS analysis of the NW-1 apatite yielded a slightly discordant age around 1160 Ma, which is verified by SIMS analysis. In addition, laser ablation of calzirtite in NW-1 gives a ^{207}Pb–^{206}Pb age of 1170 ± 11 Ma, which is identical within analytical error to the ^{207}Pb–^{206}Pb age of 1159 ± 5 Ma given by SIMS analysis (Wu *et al.* 2010). Laser ablation of the NW-4 apatite gives an intercept age of 1166 ± 28 Ma. If all these ages are considered together, a mean age of 1158 ± 3 Ma is obtained, which is identical to the TIMS age of baddeleyite/zircon by Rukhlov & Bell (2010).

For the ijolitic rocks, baddeleyite from MT25 gives an age of 1169 ± 22 Ma. The large error is owing to the extremely low concentration of uranium (less than 5 ppm), and hence low signal during analysis. Fortunately, an ijolitic clast (P10L) within the carbonatite gives a more precise age of 1164 ± 4 Ma, which is identical to those obtained from the carbonatite. Therefore, it can be concluded that the Prairie Lake complex was emplaced at ~1160 Ma.

5.b. Emplacement age relative to Midcontinent Rift magmatism

Midcontinent rifting was accompanied by numerous stages of magmatism. According to Heaman *et al.* (2007), four stages of magmatism can be identified. Stage 1 (1150–1130 Ma) magmatism, interpreted as the earliest manifestation of Midcontinent rifting, is represented by numerous lamprophyre dykes and minor felsic volcanic rocks, which are temporally related to the well-known Abitibi dyke swarm (1141 Ma, Ernst & Buchan, 1997; Heaman *et al.* 2007). Stage 2 (1115–1105 Ma), the onset of the Midcontinent rifting, is represented by diverse ultramafic intrusions, basaltic sills and flows, rhyolites and alkaline rocks. Stage 3 (1100–1094 Ma) is the main period of Midcontinent rifting, and is represented by mafic intrusions (Duluth Complex) and basalt flows, with minor amounts of alkaline rocks (Lackner Lake carbonatite). Stage 4 (<1094 Ma) represents the waning stage of the Midcontinent rifting, and is expressed by porphyry and basaltic dykes.

The alkaline rock and carbonatite complexes within the rift area are mostly considered to belong to stage 2 magmatism (Heaman *et al.* 2007). However, the available geochronological data indicate that the alkaline magmatism extends over a significant time interval (Heaman & Machado, 1992; Heaman *et al.* 2007; Rukkhlov & Bell, 2010; and this study). For the complexes within the Kapuskasing Structural Zone, the complexes include Firesand River (1139.7 ± 2.5 Ma), Valentine Township (1114.7 ± 1.1 Ma), Nemogosenda (1105.4 ± 2.6 Ma) and Lackner Lake (1100.6 ± 1.5 Ma). Within the Trans-Superior Tectonic Zone, only Prairie Lake (1158 ± 3 Ma) and Coldwell (1107 ± 2 to 1109 ± 8 Ma) have reliable age determinations. In addition to complexes within the two main tectonic zones, carbonatite complexes are found at Big Beaver House (1093.0 ± 1.7 Ma) and Schryburt Lake (1083.5 ± 2.9 Ma) to the northwest of these zones (Fig. 1). Thus, the ages of the alkaline rock and carbonatite magmatism range from 1158 to 1084 Ma, indicating that such magmatism occurred during all stages of the Midcontinent rifting.

The range of age determinations can be interpreted as either reflecting magmatism associated with passive continental rifting or that associated with the initial stages of plume-induced rifting. If these complexes were related to mantle plume activity, then the lifetime of this plume must be as long as >70 Ma (Heaman *et al.* 2007; Hollings, Smyk & Cousens, 2012). It is also noted, from these age data, that the Prairie Lake complex is the oldest alkaline–carbonatite complex associated with the Midcontinent rifting. Detailed discussion of the merits of passive versus active rifting in the genesis of the Midcontinent Rift is well beyond the scope of this work. Our data have no direct bearing on whether the emplacement of the Prairie Lake complex was related to crustal extension and passive rifting or an upwelling mantle plume. Our data merely indicate that the earliest manifestation of magmatism in this region was at 1160 Ma. If this was related to plume activity then the plume activity would extend from 1160 to 1094 Ma. In support of a plume-related origin, Sasada *et al.* (1997) found that apatite from Prairie Lake has an extremely high $^{136}Xe/^{130}Xe$ ratio and excess ^{129}Xe, and suggested that it might be related to less-degassed primordial mantle, which is comparable to a proposed plume model (Bell & Simonetti, 2010; Ernst & Bell, 2010).

It has been proposed that the Prairie Lake complex is spatially and age-related to the nearby large alkaline complexes, and that these complexes represent differentiated segments of magma that travelled on different paths, but that have been generated from the same magma source (Gittins, Macintyre & York, 1967). However, from the geochronological data presented here, the Prairie Lake complex was emplaced much earlier than the Coldwell and Killala complexes. Other petrological studies indicate that these A-type granitoid complexes such as the Coldwell complex (Mitchell *et al*. 1993), lacking carbonatite, are derived by partial melting of metasomatized lower crust (Martin, 2006). Therefore, those complexes are not genetically related to the Prairie Lake carbonatite complex.

https://doi.org/10.1017/S0016756815001120 Published online by Cambridge University Press

5.c. Aspects of the petrogenesis of the Prairie Lake complex

It is not an objective of this paper to discuss the petrogenesis of the Prairie Lake complex as this is beyond the scope of this work. However, our new isotopic data do have a bearing on this problem and are commented on below.

The petrogenesis of alkaline rock and carbonatite complexes remains one of the major unresolved problems in petrology (Bell, 1998; Harmer & Gittins, 1998; Harmer, 1999). It is commonly suggested that nepheline-bearing rocks and carbonatites can be related by fractional crystallization or liquid immiscibility to a common parental magma. Typically, evidence for immiscibility is circumstantial and the hypothesis is based primarily on extrapolation of laboratory studies of synthetic haplocarbonatites (Lee & Wyllie, 1998; Kjarsgaard, 1998; Brooker & Kjarsgaard, 2011; Martin *et al.* 2013), and/or experimental geochemical studies (Jones *et al.* 1995; Veksler *et al.* 1998, 2012) rather than direct petrographic or geological evidence for the process. For example, conjugate liquids as represented by melt inclusions have not been described from ijolite–carbonatite complexes, although conjugate immiscible melt pairs have been observed for wollastonite nephelinite and natrocarbonatite (Mitchell, 2009; Mitchell & Dawson, 2012).

The major observations stemming from this work are that: (1) All of the rock units occurring at Prairie Lake were emplaced contemporaneously within the resolution of the age determinations at ~1160 Ma; (2) All the rocks have effectively identical initial Sr and Nd isotopic compositions, indicating derivation from a common parental magma. To our knowledge, the Prairie Lake complex has the most homogeneous isotopic composition of any carbonatitic complex. Our data certainly do not support the contentions of Gittins & Harmer (2003) that the relationships between silicate and carbonatite rocks within alkaline complexes is spatial rather then genetic; (3) None of the rocks exhibit isotopic evidence for significant contamination by crustal material.

None of these isotopic data provide conclusive evidence for any particular petrogenetic scheme and must be considered in conjunction with geological evidence. However, geological observations suggest that the Prairie Lake plutonic and hypabyssal rocks formed within a continuously replenished, continuously fractionating magma chamber beneath a nephelinitic volcano. Consequently, there are several distinct episodes of ijolite and carbonatite formation in addition to cumulate formation and disaggregation. There is petrographic evidence for fractional crystallization and magma mixing in many of the ijolites and carbonatites but no evidence for liquid immiscibility. That the Prairie Lake rocks appear to have crystallized from a very homogeneous magma is either a consequence of these mixing processes or derivation from a homogeneous source. The details of the petrogenesis will be presented in a subsequent paper.

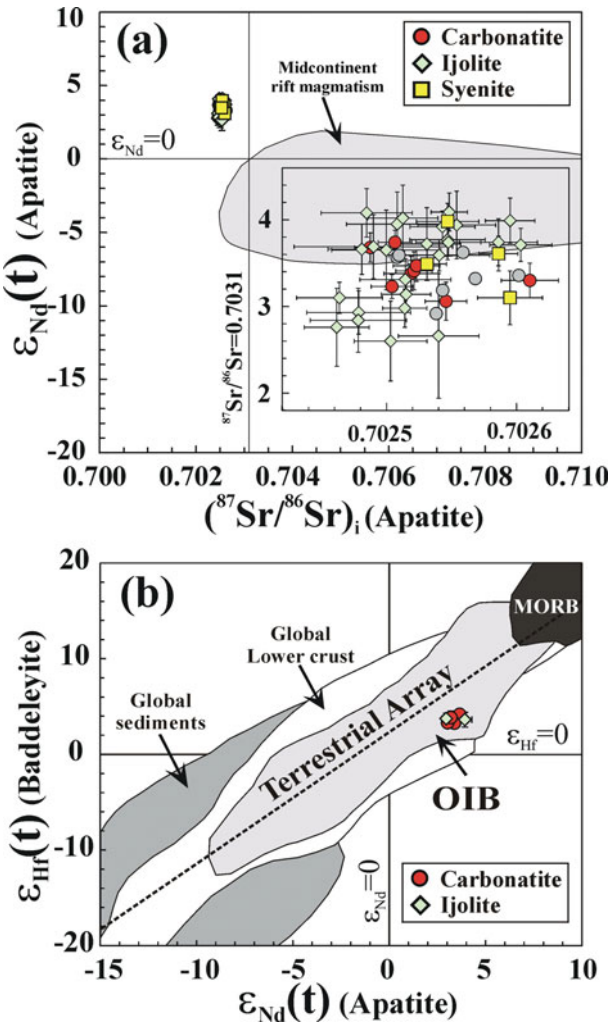

Figure 10. (Colour online) (a) Sr–Nd and (b) Nd–Hf isotopic variations of the Prairie Lake complex. Sr–Nd literature data for the complex (grey circles in (a)) are from S. J. Pollock (unpub. MSc thesis, Carleton Univ., 1987), and Midcontinent Rift magmatism is from Hollings, Smyk & Cousens (2012). The fields of MORB (mid-ocean ridge basalt), OIB (ocean island basalt), global lower crust and sediments in (b) are from Wu *et al.* (2011).

5.d. Isotopic heterogeneity of the mantle source of the Midcontinent magmatism

It was determined in this study that the ijolite, syenite and carbonatite from the Prairie Lake complex show identical Sr–Nd isotopic compositions (Fig. 10a). The ijolite has an initial $^{87}Sr/^{86}Sr$ ratio of ~0.70254 and a positive $\varepsilon_{Nd}(t)_{1160}$ value of +3.5, and the syenite has the above values of ~0.70257 and +3.6. Similarly, the carbonatite has a $^{87}Sr/^{86}Sr$ ratio of ~0.70252 and $\varepsilon_{Nd}(t)_{1160}$ value of +3.4. In addition, baddeleyites from the ijolite and carbonatite have identical Hf isotopic compositions (Table 4), and the Nd–Hf isotopic correlation indicates that these rocks have a similar isotopic composition to that of oceanic island basalt (OIB; Fig. 10b). In agreement with Bell & Blenkinsop (1987), Rukhlov & Bell (2010) and (Rukhlov, Bell & Amelin, 2015), we conclude that the silicate and carbonatitic magmas are derived from a weakly depleted mantle source that was formed at 3 Ga ago. Our data fit the Sr and Nd

https://doi.org/10.1017/S0016756815001120 Published online by Cambridge University Press

development lines for such a source as given by Rukhlov, Bell & Amelin (2015).

Available data indicate that the igneous rocks formed during the Midcontinent rifting have variable isotopic compositions (Paces & Bell, 1989; Nicholson & Shirey, 1990; Lightfoot, Sutcliffe & Doherty, 1991; Shirey *et al.* 1994; Nicholson *et al.* 1997; Hollings *et al.* 2007; Hollings, Smyk & Cousens, 2012; Bright *et al.* 2014). For example, the vast majority of basalt in the rift is quite uniform with $\varepsilon_{Nd}(t)$ values ranging between −2.5 and +3.5. If only primitive olivine tholeiites are considered, then an even more restricted range of −0.3 to +0.8 is observed (Paces & Bell, 1989). Similarly, the younger (~1100–1094 Ma) volcanic rocks also have a positive $\varepsilon_{Nd}(t)$ value of +1 to +4 (Nicholson *et al.* 1997). In contrast, the 1110–1120 Ma mafic sills in the Nipigon Embayment and Thunder Bay to the west of the studied area have negative $\varepsilon_{Nd}(t)$ values of +0.9 to −9.3 with initial $^{87}Sr/^{86}Sr$ ratios of 0.7032 to 0.7243 (Hollings *et al.* 2007; Hollings, Smyk & Cousens, 2012), indicating their derivation from ancient subcontinental lithospheric enriched mantle or contamination by crustal material during their crystallization.

As for the alkaline complexes, Heaman & Machado (1992) reported that gabbro from the Coldwell complex has $\varepsilon_{Nd}(t)$ values of −2.6 to +1.6 with initial $^{87}Sr/^{86}Sr$ ratios of 0.70336 to 0.70349, whereas syenites have the above values of −0.5 to −4.6 with initial $^{87}Sr/^{86}Sr$ ratios of 0.70361 to 0.70416, slightly different from the Prairie Lake complex. However, Bell & Blenkinsop (1987, 1989) found a large Sr–Nd isotopic variation for other alkaline–carbonatitic complexes, such as Nemegosenda, Big Heaver House, Firesand River, Clay-Howells, Seabrook and Schryburt Lake. The Nemegosenda and Clay-Howells complexes have initial $^{87}Sr/^{86}Sr$ ratios of 0.7037 and $\varepsilon_{Nd}(t)$ values of −2.1 to +0.6, and thus are similar to the Coldwell complex, whereas other complexes have $^{87}Sr/^{86}Sr$ ratios of 0.7024 to 0.7026 and $\varepsilon_{Nd}(t)$ values of +2.4 to +3.6, similar to the Prairie Lake complex. This variable isotopic composition among the different kinds of rock suggests that the mantle magmatism had a complex relationship between the mantle and crust. Alternatively, these rocks derived from a heterogeneous mantle source, as proposed by Kwon, Tilton & Grüenenfelder (1989) and Tilton & Kwon (1990). Although no isotopic data are available for the Killala and Chipman Lake complexes, it could be concluded that at least some alkaline–carbonatite complexes in the area (Prairie Lake, Big Heaver House, Firesand River, Seabrook and Schryburt Lake) have the most depleted mantle composition among the various rocks formed during the Midcontinent rifting.

6. Conclusions

Comprehensive age determinations and Sr–Nd–Hf isotopic analyses of baddeleyite, apatite, calcite, titanite and perovskite from the Prairie Lake complex in Ontario, Canada, lead to the following conclusions:

(1) Baddeleyite from the carbonatite and ijolite, and apatite from the carbonatite yield identical U–Pb ages of ~1160 Ma, indicating that the different phases of the complex were emplaced contemporaneously;

(2) Sr–Nd–Hf isotopic analyses of apatite, calcite, titanite, perovskite and baddeleyite indicate that the different rock types of the complex do not show any significant isotopic variation, indicating that the silicate and carbonate rocks are co-genetic and originate from a single magma type by simple crystal fractionation. The low $^{87}Sr/^{86}Sr$ ratio of ~0.70254 and positive $\varepsilon_{Nd}(t)_{1160}$ and $\varepsilon_{Hf}(t)_{1160}$ values of ~+3.5 and +4.6 suggest that the complex was derived from a weakly depleted mantle;

(3) The U–Pb data have reinforced the previous conclusion that the Prairie Lake complex is one of the earliest manifestations of Midcontinent magmatism, and this complex was not formed contemporaneously with other alkaline complexes in the area (Coldwell, Killala).

Acknowledgements. Yang Li, Liang-Liang Zhang and Wei-Qiang Ji are thanked for their assistance during sample preparation and analyses. Kevin R. Chamberlain and Yuri Amelin helped to run the TIMS analyses for the NW-1 apatite. Peter Hollings and Shannon Zurevinski read the early draft and provided invaluable comments on the characters of the Midcontinent Rift and carbonatite petrogenesis. Constructive reviews by Keith Bell, Shannon Zurevinski, Tony Simonetti and anonymous reviewers greatly improved the manuscript. This work was supported by the Natural Science Foundation of China (Grant 41130313). Roger Mitchell's work on alkaline rocks and carbonatites is supported by the Natural Sciences and Engineering Research Council of Canada, Almaz Petrology and Lakehead University. Paul Jones of Nuinsco Resources is thanked for access to their exploration properties at Prairie Lake.

Supplementary material

To view supplementary material for this article, please visit http://dx.doi.org/10.1017/S0016756815001120.

References

BELL, K. 1998. Radiogenic isotope constraints on relationships between carbonatites and associated silicate rocks – a brief review. *Journal of Petrology* **39**, 1987–96.

BELL, K. & BLENKINSOP, J. 1980. Ages and initial $^{87}Sr/^{86}Sr$ ratios from alkalic complexes of Ontario. In *Geoscience Research Grant Program, Summary of Research 1979–1980* (ed. E. G. Pye), pp. 16–23. Ontario Geological Survey Miscellaneous Paper 93.

BELL, K. & BLENKINSOP, J. 1987. Archean depleted mantle: evidence from Nd and Sr initial isotopic ratios of carbonatites. *Geochimica et Cosmochimica Acta* **51**, 291–8.

BELL, K. & BLENKINSOP, J. 1989. Neodymium and strontium isotope geochemistry of carbonatites. In *Carbonatites: Genesis and Evolution* (ed. K. Bell), pp. 278–300. London: Unwin Hyman.

BELL, K., BLENKINSOP, J., COLE, T. J. S. & MENAGH, D. P. 1982. Evidence from Sr isotopes for long-lived heterogeneities in the upper mantle. *Nature* **298**, 251–3.

BELL, K. & SIMONETTI, A. 2010. Source of parental melts to carbonatites – critical isotopic constraints. *Mineralogy and Petrology* **98**, 77–89.

BOTTRIELL, K. J. 1975. *Rubidium–strontium isochron age studies of Nemegosenda and Prairie Lake*. B. Sc. thesis, Carleton University, Ottawa, Canada, **44** pp. Published thesis.

BRIGHT, R. M., AMATO, J. M., DENYSZYN, S. W. & ERNST, R. E. 2014. U–Pb geochronology of 1.1 Ga diabase in the southwestern United States: testing models for the origin of a post-Grenville large igneous province. *Lithosphere* **6**, 135–56.

BROOKER, R. A. & KJARSGAARD, B. A. 2011. Silicate-carbonate liquid immiscibility and phase relations in the system SiO_2–Na_2O–Al_2O_3–CaO–CO_2 at 0.1–2.5 GPa with applications to carbonatite genesis. *Journal of Petrology* **52**, 1281–305.

BURKE, K. & DEWEY, K. L. 1973. Plume generated triple junctions: key indicators in applying plate tectonics to old rocks. *Journal of Geology* **81**, 406–33.

CANNON, W. F. 1992. The North American Midcontinent Rift beneath the Lake Superior region with emphasis on its geodynamic evolution. *Tectonophysics* **213**, 41–8.

ERNST, R. E. & BELL, K. 2010. Large igneous provinces (LIPs) and carbonatites. *Mineralogy and Petrology* **98**, 55–76.

ERNST, R. & BLEEKER, W. 2010. Large igneous provinces (LIPs), giant dyke swarms, and mantle plumes: significance for breakup events within Canada and adjacent regions from 2.5 Ga to the present. *Canadian Journal of Earth Sciences* **47**, 695–739.

ERNST, R. E. & BUCHAN, K. L. 1997. Giant radiating dyke swarms: their use in identifying pre-Mesozoic large igneous provinces and mantle plumes. In *Large Igneous Provinces: Continental, Oceanic, and Planetary Flood Volcanism* (eds J. Mahoney & M. Coffin), pp. 297–333. American Geophysical Union, Geophysical Monograph vol. 100. Washington, DC, USA.

FISHER, C. M., VERVOORT, J. D. & DUFRANE, S. A. 2014. Accurate Hf isotope determinations of complex zircons using the "laser ablation split stream" method. *Geochemistry, Geophysics, Geosystems* **15**, 121–39.

GITTINS, J. & HARMER, R. E. 2003. Myth and reality in the carbonatite – silicate rock "association". *Periodico di Mineralogia* **72**, 19–26.

GITTINS, J., MACINTYRE, R. M. & YORK, D. 1967. The ages of carbonatite complexes in eastern Canada. *Canadian Journal of Earth Sciences* **4**, 651–5.

GRIFFIN, W. L., POWELL, W. J., PEARSON, N. J. & O'REILLY, S. Y. 2008. GLITTER: data reduction software for laser ablation ICP–MS. In *Laser Ablation-ICP–MS in the Earth Sciences: Current Practices and Outstanding Issues* (ed. P. Sylvester), pp. 308–11. Mineralogical Association Canada Short Course no. 40.

HARMER, R. E. 1999. The petrogenetic association of carbonatite and alkaline magmatism: constraints from the Spitskop Complex, South Africa. *Journal of Petrology* **40**, 525–48.

HARMER, R. E. & GITTINS, J. 1998. The case for primary, mantle-derived carbonatite magma. *Journal of Petrology* **39**, 1895–903.

HEAMAN, L. M. 2009. The application of U–Pb geochronology of mafic, ultramafic and alkaline rocks: an evaluation of three mineral standards. *Chemical Geology* **261**, 42–51.

HEAMAN, L. M., EASTON, R. M., HART, T. R., HOLLINGS, P., MACDONALD, C. A. & SMYK, M. 2007. Further refinement to the timing of Mesoproterozoic magmatism, Lake Nipigon region, Ontario. *Canadian Journal of Earth Sciences* **44**, 1055–86.

HEAMAN, L. M. & MACHADO, N. 1992. Timing and origin of Midcontinent Rift alkaline magmatism, North America: evidence from the Coldwell Complex. *Contributions to Mineralogy and Petrology* **110**, 289–303.

HOLLINGS, P., RICHARDSON, A., CREASER, R. & FRANKLIN, J. 2007. Radiogenic isotope characteristics of the Mid-proterozoic intrusive rocks of the Nipigon Embayment, Northwestern Ontario. *Canadian Journal of Earth Sciences* **44**, 1111–29.

HOLLINGS, P., SMYK, M. & COUSENS, B. 2012. The radiogenic isotope characteristics of dikes and sills associated with the Mesoproterozoic Midcontinent Rift near Thunder Bay, Ontario, Canada. *Precambrian Research* **214/215**, 269–79.

JONES, J. H., WALKER, D., PICKET, D. A., MURREL, M. T. & BEATE, P. 1995. Experimental investigations of the partitioning of Nb, Mo, Ba, Ce, Pb, Ra, Th, Pa and U between immiscible carbonate and silicate liquids, *Geochimica et Cosmochimica Acta* **59**, 1307–20.

KEMP, A. I. S., FOSTER, G. L., SCHERSTEN, A., WHITEHOUSE, M. J., DARLING, J. & STOREY, C. 2009. Concurrent Pb–Hf isotope analysis of zircon by laser ablation multi-collector ICP-MS, with implications for the crustal evolution of Greenland and the Himalayas. *Chemical Geology* **261**, 244–60.

KIMURA, J. I., TANI, K. & CHANG, Q. 2012. Determination of Hf isotope ratios in zircon using multiple collector-inductively coupled plasma mass spectrometry equipped with laser ablation and desolvating nebulizer dual sample introduction system. *Geochemical Journa*l **46**, 1–12.

KJARSGAARD, B. A. 1998. Phase relations of a carbonated high-CaO nephelinite at 0.2 and 0.5 GPa. *Journal of Petrology* **39**, 2061–75.

KRASNOVA, N. I., PETROV, T. G., BALAGANSKAYA, E. G., GARCIA, D., MOUTTE, J., ZAITSEV, A. N. & WALL, F. 2004. Introduction to phoscorites: occurrence, composition, nomenclature and petrogenesis. In *Phoscorites and Carbonatites from Mantle to Mine: The Key Example of the Kola Alkaline Province* (eds F. Wall & A. N. Zaitsev), pp. 43–72. Mineralogical Society Series no. 10.

KWON, S. T., TILTON, G. R. & GRÜENENFELDER, M. H. 1989. Lead isotope relationships in carbonatites and alkalic complexes: an overview. In *Carbonatites: Genesis and Evolution* (ed. K. Bell), pp. 360–87. London: Unwin Hyman.

LEE, W. J. & WYLLIE, P. J. 1998. Processes of crustal carbonatite formation by liquid immiscibility and differentiation, elucidated by model systems. *Journal of Petrology* **39**, 2005–13.

LI, Q. L., LI, X. H., LIU, Y., TANG, G. Q., YANG, J. H. & ZHU, W. G. 2010. Precise U–Pb and Pb–Pb dating of Phanerozoic baddeleyite by SIMS with oxygen flooding technique. *Journal of Analytical Atomic Spectrometry* **25**, 1107–13.

LI, Q. L., LI, X. H., WU, F. Y., YIN, Q. Z., YE, H. M., LIU, Y., TANG, G. Q. & ZHANG, C. L. 2012. *In-situ* SIMS U–Pb dating of Phanerozoic apatite with low U and high common Pb. *Gondwana Research* **21**, 745–56.

LIGHTFOOT, P., SUTCLIFFE, R. & DOHERTY, W. 1991. Crustal contamination identified in Keweenawan Osler Group tholeiites, Ontario: a trace element perspective. *Journal of Geology* **99**, 739–60.

LUDWIG, K. R. 2003. *ISOPLOT 3.0 – A Geochronological Toolkit for Microsoft Excel*. Berkeley Geochronology Center Special Publication, No. 4, 70 pp.

MARIANO, A. N. 1979. *Report of the geology and economic potential of the Prairie Lake carbonatite-alkalic complex*. 18 pp.

MARIANO, A. N. & ROEDER, P. L. 1989. Wöhlerite: chemical composition, cathodoluminescence and environment of crystallization. *The Canadian Mineralogist* **27**, 709–20.

MARTIN, R. F. 2006. A-type granites of crustal origin ultimately result from open-system fenitization-type reactions in an extensional environment. *Lithos* **91**, 125–36.

MARTIN, L. H. J., SCHMIDT, M. W, MATTSSON, H. B. & GUENTHER, D. 2013. Element partitioning between immiscible carbonatite and silicate melts for dry and H_2O-bearing systems at 1–3 GPa. *Journal of Petrology* **54**, 2301–38.

MCFARLANE, C. R. M. & MCCULLOCH, M. T. 2007. Coupling of in-situ Sm/Nd systematics and U/Pb dating of monazite and allanite with applications to crustal evolution studies. *Chemical Geology* **245**, 45–60.

MERINO, M., KELLER, G. R., STEIN, S. & STEIN, C. 2013. Variations in Mid-continent rift magma volumes consistent with microplate evolution. *Geophysical Research Letters* **40**, 1513–6.

MITCHELL, R. H. 2009. Peralkaline nephelinite–natrocarbonatite immiscibility and carbonatite assimilation at Oldoinyo Lengai, Tanzania. *Contributions to Mineralogy and Petrology* **158**, 589–98.

MITCHELL, R. H. & DAWSON, J. B. 2012. Carbonate-silicate immiscibility and extremely peralkaline silicate glasses from Nasira cone and recent eruptions at Oldoinyo Lengai Volcano, Tanzania. *Lithos* **152**, 40–6.

MITCHELL, R. H. & PLATT, R. G. 1978. Mafic mineralogy of ferroaugite syenite from the Coldwell alkaline complex, Ontario, Canada. *Journal of Petrology* **19**, 627–51.

MITCHELL, R. H. & PLATT, R. G. 1979. Nepheline-bearing rocks from the Poohbah Lake complex, Ontario: malignites and malignites. *Contributions to Mineralogy and Petrology* **69**, 255–64.

MITCHELL, R. H., PLATT, R. G. & CHEADLE, S. P. 1983. A gravity study of the Coldwell complex, northwestern Ontario and its petrological significance. *Canadian Journal of Earth Sciences* **20**, 1631–8.

MITCHELL, R. H., PLATT, R. G., LUKOSIUS-SANDERS, J., ARTIST-DOWNEY, M. & MOOGK-PICKARD, S. 1993. Petrology of syenites from center III of the Coldwell alkaline complex, northwestern Ontario, Canada. *Canadian Journal of Earth Sciences* **30**, 145–58.

MOREL, M. L. A., NEBEL, O., NEBEL-JACOBSEN, Y. J., MILLER, J. S. & VROON, P. Z. 2008. Hafnium isotope characterization of the GJ-1 zircon reference material by solution and laser-ablation MC–ICPMS. *Chemical Geology* **255**, 231–5.

NICHOLSON, S. W. & SHIREY, S. B. 1990. Midcontinent Rift volcanism in the Lake Superior Region: Sr, Nd and Pb isotopic evidence for a mantle plume origin. *Journal of Geophysical Research* **95**, 10851–68.

NICHOLSON, S. W., SHIREY, S., SCHULZ, K. & GREEN, J. 1997. Rift-wide correlation of 1.1 Ga Midcontinent rift system basalts: implications for multiple mantle sources during rift development. *Canadian Journal of Earth Sciences* **34**, 504–20.

PACES, J. B. & BELL, K. 1989. Non-depleted sub-continental mantle beneath the Superior Province of the Canadian Shield: Nd–Sr isotopic and trace element evidence from Midcontinent Rift basalts. *Geochimica et Cosmochimica Acta* **53**, 2023–35.

PACES, J. B. & MILLER JR, J. D. 1993. Precise U–Pb ages of Duluth Complex and related mafic intrusions, northeastern Minnesota: geochronological insights to physical, petrogenetic, paleomagnetic, and tectonomagmatic processes associated with the 1.1 Ga Midcontinent Rift System. *Journal of Geophysical Research* **98**, 13997–4013.

PALMER, H. C. & DAVIS, D. W. 1987. Paleomagnetism and U–Pb geochronology of volcanic rocks from Michipicoten Island, Lake Superior, Canada: precise calibration of the Keweenawan polar wander track. *Precambrian Research* **37**, 157–71.

PLATT, R. G. & WOOLLEY, A. R. 1990. The carbonatites and fenites of Chipman Lake, Ontario. *The Canadian Mineralogist* **28**, 241–50.

PURTICH, E., ARMSTRONG, T. & YASSA, A. 2010. *Technical Report on the Prairie Lake Property, Thunder Bay Mining Division, Ontario, Canada*. NI 43–101 Technical Report, 109 pp.

RUKHLOV, A. S. & BELL, K. 2010. Geochronology of carbonatites from the Canadian and Baltic shields, and the Canadian Cordillera: clues to mantle evolution. *Mineralogy and Petrology* **98**, 11–54.

RUKHLOV, A. S., BELL, K, & AMELIN, Y. 2015. Carbonatites, isotopes and evolution of the subcontinental mantle: an overview. In *Symposium on Strategic and Critical Materials* (eds G. J. Simandl & M. Neetz), pp. 39–64. British Columbia Geological Survey Paper 2015-3.

SAGE, R. P. 1983. *Geology of the Prairie Lake Carbonatite Complex. Ontario*. Geological Survey Open File Report, 5412, 133 pp.

SAGE, R. P. 1987. *Geology of Carbonatite—Alkalic Rock Complexes in Ontario: Prairie Lake Carbonatite Complex, District of Thunder Bay*. Ministry of Northern Development and Mines, Ontario Geological Survey, Study 46, 91 pp.

SANO, Y., OYAMA, T., TERADA, K. & HIDAKA, H. 1999. Ion microprobe U–Pb dating of apatite. *Chemical Geology* **153**, 249–58.

SASADA, T., HIYAGON, H., BELL, K. & EBIHARA, M. 1997. Mantle-derived noble gases in carbonatites. *Geochimica et Cosmochimica Acta* **61**, 4219–28.

SHIREY, S., KLEWIN, K., BERG, J. & CARLSON, R. 1994. Temporal changes in the sources of flood basalts: isotopic and trace element evidence from the 1100 Ma old Keweenawan Mamainse Point Formation, Ontario, Canada. *Geochimica et Cosmochimica Acta* **58**, 4475–90.

STACEY, J. S. & KRAMERS, J. D. 1975. Approximation of terrestrial lead isotope evolution by a two-stage model. *Earth and Planetary Science Letters* **26**, 207–21.

TAPPE, S., FOLEY, S. F., STRACKE, A., ROMER, R. L., KJARSGAARD, B. A., HEAMAN, L. M. & JOYCE, N. 2007. Craton reactivation on the Labrador Sea margins: $^{40}Ar/^{39}Ar$ age and Sr–Nd–Hf–Pb isotope constraints from alkaline and carbonatite intrusives. *Earth and Planetary Science Letters* **256**, 433–54.

TILTON, G. R. & KWON, S. T. 1990. Isotopic evidence for crust-mantle evolution with emphasis on the Canadian Shield. *Chemical Geology* **83**, 149–83.

VAN SCHMUS, W. R. & HINZE, W. J. 1985. The midcontinent rift system. *Annual Review of Earth and Planetary Sciences* **13**, 345–83.

VEKSLER, I. V., DORFMAN, A. M., DULSKI, P., KAMENETSKY, V. S., DANYUSHEVSKY, L. V., JEFFRIES, T. & DINGWELL, D. B. 2012. Partitioning of elements between silicate melt and immiscible fluoride, chloride, carbonate, phosphate and sulfate melts, with implications to the origin of natrocarbonatite. *Geochimica et Cosmochimica Acta* **79**, 20–40.

https://doi.org/10.1017/S0016756815001120 Published online by Cambridge University Press

VEKSLER, I.V., PETIBON, C., JENNER, G. A., DORFMAN, A. M. & DINGWELL, D. B. 1998. Trace element partitioning in immiscible silicate–carbonate liquid systems: an initial experimental study using a centrifuge autoclave. *Journal of Petrology* **39**, 2095–104.

VERVOORT, J. D., WIRTH, K., KENNEDY, B., SANDLAND, T. & HARPP, K. S. 2007. The magmatic evolution of the Midcontinent rift: new geochronologic and geochemical evidence from felsic magmatism. *Precambrian Research* **157**, 235–68.

WINDLEY, B. F. 1993. Proterozoic anorogenic magmatism and its orogenic connections. *Journal of Geological Society, London* **150**, 39–50.

WINGATE, M. T. D. & COMPSTON, W. 2000. Crystal orientation effects during ion microprobe U–Pb analysis of baddeleyite. *Chemical Geology* **168**, 75–97.

WOODHEAD, J. D. & HERGT, J. M. 2005. A preliminary appraisal of seven natural zircon reference materials for in-situ Hf-isotope analysis. *Geostandards and Geoanalytical Research* **29**, 183–95.

WU, F. Y., ARZAMASTSEV, A. A., MITCHELL, R. H., LI, Q. L., SUN, J., YANG, Y. H. & WANG, R. C. 2013. Emplacement age and Sr–Nd isotopic compositions of the Afrikanda alkaline ultramafic complex, Kola Peninsula, Russia. *Chemical Geology* **353**, 210–29.

WU, F. Y., YANG, Y. H., LI, Q. L., MITCHELL, R. H., DAWSON, J. B., BRAND, G. & YUHARA, M. 2011. *In situ* determination of U–Pb ages and Sr–Nd–Hf isotopic constraints on the petrogenesis of the Phalaborwa carbonatite Complex, South Africa. *Lithos* **127**, 309–22.

WU, F. Y., YANG, Y. H., MITCHELL, R. H., BELLATRECCIA, F., LI, Q. L. & ZHAO, Z. F. 2010. *In situ* U–Pb and Nd–Hf–(Sr) isotopic investigations of zirconolite and calzirtite. *Chemical Geology* **277**, 178–95.

WU, F. Y., YANG, Y. H., XIE, L. W., YANG, J. H. & XU, P. 2006. Hf isotopic compositions of the standard zircons and baddeleyites used in U–Pb geochronology. *Chemical Geology* **234**, 105–26.

YANG, Y. H., SUN, J. F., XIE, L. W., FAN, H. R. & WU, F. Y. 2008. *In situ* Nd isotopic measurements of geological samples by laser ablation. *Chinese Science Bulletin* **53**, 1062–70.

YANG, Y. H., WU, F. Y., WILDE, S. A., LIU, X. M., ZHANG, Y. B., XIE, L. W. & YANG, J. H. 2009. *In situ* perovskite Sr–Nd isotopic constraints on petrogenesis of the Mengyin kimberlites in the North China Craton. *Chemical Geology* **264**, 24–42.

YANG, Y. H., WU, F. Y., YANG, J. H., CHEW, D. M., XIE, L. W., CHU, Z. Y., ZHANG, Y. B. & HUANG, C. 2014. Sr and Nd isotopic compositions of apatite reference materials used in U–Th–Pb geochronology. *Chemical Geology* **385**, 35–55.